Article:
Robbins, LJ, Fakhraee, M, Smith, AJB et al. (2023) Manganese oxides, Earth surface oxygenation, and the rise of oxygenic photosynthesis. Earth-Science Reviews, 239. 104368. ISSN: 0012-8252

https://doi.org/10.1016/j.earscirev.2023.104368

Manganese oxides, Earth surface oxygenation, and the rise of oxygenic photosynthesis

Leslie J. Robbins[1,†], Mojtaba Fakhraee[2,3,4†], Albertus J.B. Smith[5,6], Brendan A. Bishop[1], Elizabeth D. Swanner[7], Caroline Peacock[8], Chang-Le Wang[9,10], Noah J. Planavksy[3,4], Christopher T. Reinhard[2,3], Sean A. Crowe[11,12], Timothy W. Lyons[3,13]

[1]Department of Geology, University of Regina, Regina, SK, Canada
[2]School of Earth and Atmospheric Sciences, Georgia Institute of Technology, Atlanta, GA, United States
[3]NASA Interdisciplinary Consortia for Astrobiology Research (ICAR), Alternative Earths Team
[4]Department of Earth and Planetary Sciences, Yale University, New Haven, CT, United States States
[5]Paleoproterozoic Mineralization Research Group, Department of Geology, University of Johannesburg, Johannesburg, South Africa.
[6]Department of Science and Technology-National Research Foundation Centre of Excellence for Integrated Mineral and Energy Resource Analysis, University of Johannesburg, Johannesburg, South Africa
[7]Department of Geological and Atmospheric Sciences, Iowa State University, Ames, IA, United States
[8]School of Earth and Environment, University of Leeds, Leeds, United Kingdom
[9]Key Laboratory of Mineral Resources, Institute of Geology and Geophysics, Chinese Academy of Sciences, Beijing, China
[10]University of Chinese Academy of Sciences, Beijing, China
[11]Department of Earth, Ocean, and Atmospheric Sciences, University of British Columbia, Vancouver, BC, Canada
[12]Department of Microbiology and Immunology, University of British Columbia, Vancouver, BC, Canada
[13]Department of Earth and Planetary Sciences, University of California, Riverside, CA, United States

[†]These authors contributed equally to this work.

Abstract

Oxygenic photosynthesis is arguably the most important biological innovation in Earth's history, facilitating the transition to a habitable planet for complex life. Dating the emergence of oxygenic photosynthesis, however, has proven difficult with estimates spanning a billion years. Sedimentary manganese (Mn) enrichments represent a potentially important line of evidence given the high redox potentials necessary to oxidize Mn in natural environments. However, this view has been challenged by abiotic and anaerobic Mn oxidation pathways that decouple Mn enrichments from oxygenation. With these in mind, we review Mn oxidation pathways and Mn enrichments and evaluate their relation to Earth's oxygenation. We argue that despite possible alternative pathways, shallow oxygenated seawater is a prerequisite for generating and, importantly, preserving significant sedimentary Mn enrichments (and associated geochemical signals). This implies that Mn enrichments indeed track Earth's oxygenation and oxygenic photosynthesis emerged 100s of millions of years prior to irreversible atmospheric oxygenation.

1. Introduction

Manganese (Mn) has played a critical role in shaping our knowledge of Earth's protracted oxygenation, in large part due to its inherent sensitivity to changes in ambient redox conditions and propensity to undergo phase transitions during biogeochemical cycling (Fig. 1). Some of the strongest evidence for oxygen (O_2) in the environment prior to the Great Oxidation Event (GOE), which began before ca. 2.43 Ga (Gumsley et al., 2017; Bekker et al., 2020, 2021), is the presence of massive $\delta^{13}C$-depleted Mn(II) carbonates in association with iron formations and iron-rich mudstones that are believed to have been formed through Mn(IV) reduction (e.g., Planavsky et al., 2014; Smith and Beukes, 2023; Smith et al., 2023). Similarly, isotopic fractionations (e.g., Cr, Mo,

and Fe) that are driven by the presence of Mn(IV) oxides (Crowe et al., 2013; Frei et al., 2009; Planavsky et al., 2014; Wang et al., 2022) provide indirect evidence for ambient, local O_2 at least ~500 Myrs prior to the onset of the GOE (Warke et al., 2020). Some of these isotopic signals (e.g., Cr) may have been generated by more recent weathering (Albut et al., 2018; Heard et al., 2021), highlighting the need for additional robust proxies. For many years the Kalahari Mn deposit in the Hotazel Formation, South Africa, which hosts massive Mn-ore deposits, was viewed as unequivocal evidence for pervasive environmental oxygenation (e.g., Johnson et al., 2013; Tsikos et al., 2010) thus anchoring the GOE to the date of Mn deposition in the Hotazel Formation. A recent study on the mafic volcanic rocks of the underlying Ongeluk Formation places the age of the Hotazel Formation closer to 2.4 Ga (Gumsley et al., 2017). Linking deposition of the Hotazel Formation to the GOE serves as an example of how knowledge regarding the connections between ambient environmental conditions, the biosphere, and the formation of Mn deposits has the potential to inform our understanding regarding Earth's oxidation.

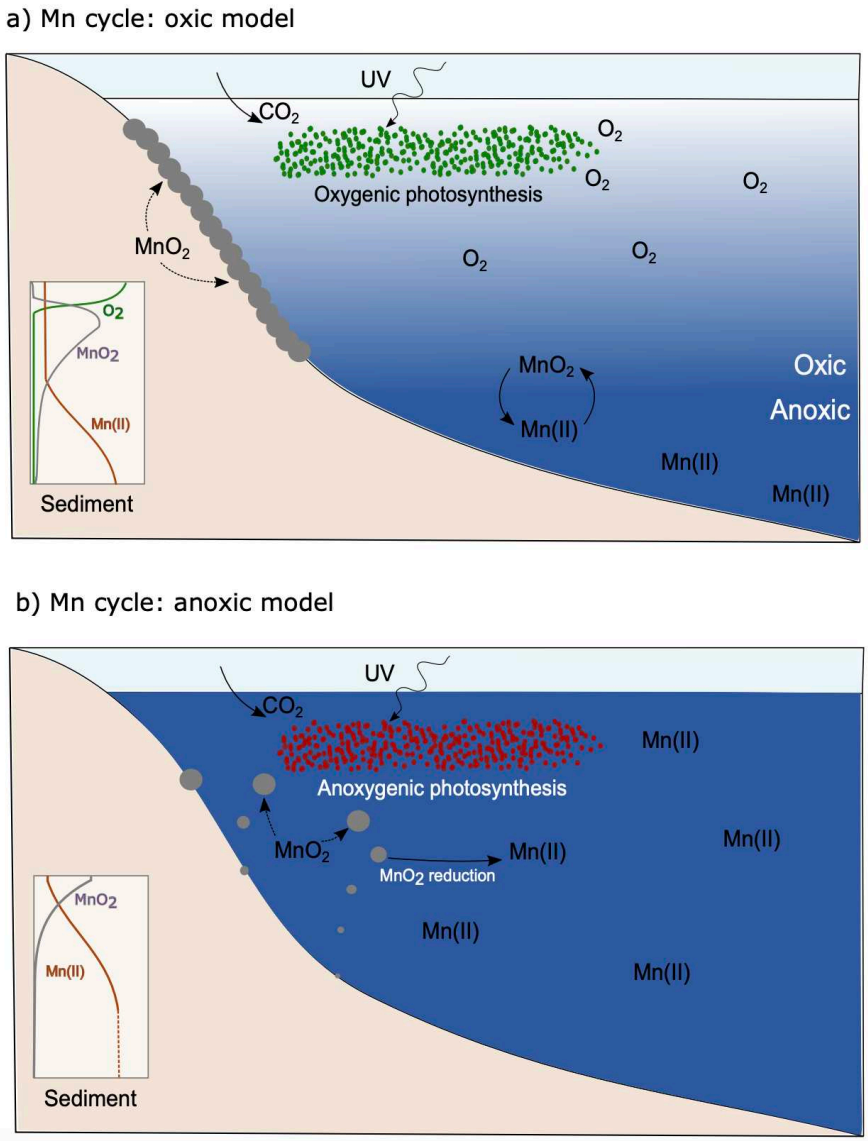

Figure 1. Schematic illustration of the manganese cycle. (A) Manganese cycling under oxic conditions, where O_2 produced by cyanobacteria in the photic zone leads to the deposition of Mn(IV) oxides. (B) Anoxic manganese cycling, where Mn(II) is oxidized by either anoxygenic photosynthetic bacteria or UV photooxidation. Inset in both models is the expected pore water chemistry profile, with a higher preservation potential for Mn(IV) oxides in A.

While the evidence is increasingly pointing to the emergence of oxygenic photosynthesis sometime in the Archean, by the onset of the Paleoproterozoic, evidence for free oxygen in Earth's surface environments becomes less controversial. For instance, enrichments in redox-sensitive

elements (RSE) such as rhenium and molybdenum, which require oxidative weathering for their generation, have been documented in the 2.5 Ga Mt. McRae Shale, Western Australia (Anbar et al., 2007). These RSE enrichments appear to be robust, reflecting primary signals, as supported by an unperturbed Re-Os age of 2495 ± 14 Ma, indicating that the system has been not altered or reset by post-depositional processes (Kendall et al., 2015). Yet, even signals such as this, which appear to be generally well constrained remain the subject of debate and ongoing investigation. For instance, Slotznick et al. (2022) presented sedimentological observations in combination with synchrotron x-ray spectroscopy images and sulfur isotope data to argue for fluid migration and subsequent oxidative weathering in the generation of RSE enrichments in the 2.5 Ga Mt. McRae Shale. Such debate highlights the lack of consensus in reconstructing the history of Earth's oxygenation and the room for additional work.

The most convincing geochemical evidence for the presence of O_2 in the environment remains the disappearance of sulfur mass-independent fractionations (S-MIF) (Farquhar et al., 2011, 2000). However, S-MIF is an atmospheric signal, and O_2 produced in the oceans was likely scavenged by marine and atmospheric sinks – reduced species – prior to the onset of the GOE. The disappearance of S-MIF occurred during the GOE, when O_2 in the atmosphere may have risen to a substantial fraction of the 21% in today's atmosphere during the Lomagundi-Jatuli Event, before returning to low to intermediate levels during the Proterozoic (Catling and Zahnle, 2020; Lyons et al., 2014; Planavsky et al., 2018). The exact timing and structure of the GOE remain an area of active discussion (G. Chen et al., 2022; Poulton et al., 2021). For instance, it is possible that O_2 levels remained elevated until at least 2.0 Ga given RSE enrichments and positively fractionated $\delta^{238}U$ recorded in the Zaonega Formation, NW Russia (Mänd et al., 2020; see Ossa Ossa et al. (2022) for an alternative view). Other recent studies have suggested that the disappearance of MIF

may have begun before the ca. 2.45-2.43 Ga (Warke et al., 2020; Bekker et al., 2020, 2021), that S-MIF signals are asynchronous between depositional basins (Philippot et al., 2018), and that O_2 may have oscillated for several hundred million years prior to the establishment of permanent atmospheric oxygenation (Bekker et al., 2020, 2021; Poulton et al., 2021). The complexity in the structure behind the rise of atmospheric O_2 and uncertainty in timing of the emergence of oxygenic photosynthesis as a metabolism capable of shaping Earth's surface environment, therefore, requires the integration of both geologic and geochemical lines of evidence.

The canonical view of large-scale Mn deposits and associated geochemical signals, including molybdenum and chromium isotope compositions and Mn/Fe ratios driven by oxidation (Crowe et al., 2013; Frei et al., 2009; Planavsky et al., 2014; Wang et al., 2022), is that they provide evidence for Archean O_2. However, there is a growing number of studies that introduce uncertainty in this paradigm. For instance, it has been suggested that Mn(II) could have been oxidized through a direct, anoxygenic photosynthetic pathway (Olson, 1970; Johnson et al., 2013) or by ultraviolet light (Liu et al., 2020), rather than by O_2 within seawater or atmosphere. To this end, recent culturing experiments have provided support for an oxygen-independent microbial pathway (Daye et al., 2019) and highlighted the potential importance of chemosynthetic Mn oxidation where electrons from Mn are coupled to carbon fixation (Yu and Leadbetter, 2020). Further challenging the requirement for O_2 in generating sedimentary Mn enrichments is recent work, suggesting that Mn(II)-enriched carbonates in the Transvaal Supergroup are the result of Mn^{2+} replacement of high-magnesium calcite precursors (Siahi et al., 2020), although this interpretation would be largely at odds with both carbon (Beukes et al., 1990; Fischer et al., 2009; although see also Tsikos et al., 2022) and iron isotopes (Johnson et al., 2008), which strongly support the diagenetic reduction of Fe and Mn during carbonate formation.

A recent increase in arguments for alternative Mn oxidation pathways that could account for the generation of substantial Mn accumulations in the absence of O_2 – anoxygenic photosynthetic pathways, photooxidation, or the direct nucleation of Mn carbonates within the water column – has spawned a new generation of discussion about the canonical interpretation of large Mn deposits. These alternative pathways for generating Mn accumulations, if fully validated ans shown to be quantitatively significant, could in principle shift our framework for viewing Mn deposits and oxygen prior to the GOE. As these new perspectives have implications for generating Mn oxides as well as carbonates, it is necessary to fully evaluate their implications for interpreting the Archean to Paleoproterozoic environment and rise of oxygenic photosynthesis. Here we review the various pathways for Mn oxidation in the environment, the conditions necessary for the preservation of Mn enrichments and the evidence for the deposition of Mn(III,IV) oxides throughout Earth's history. Furthermore, we synthesize this information in the context of a fundamental question – *Do substantial Mn carbonate deposits and associated isotopic signals prior to the Great Oxidation Event provide unambiguous evidence for the presence of free O_2 in Earth's surface environments?* We argue that the presence of shallow oxygenated seawater is a necessity for their deposition, and as such implies that the presence of significant Mn enrichments tracks the oxygenation of Earth's surface environments through time. Knowledge of the oxidative and reductive cycling of Mn on Earth, therefore, has critical implications for interpreting the geologic record of Earth's protracted oxygenation.

2. Marine Mn cycling, present, and past

As the twelfth most abundant element in Earth's crust, Mn plays an important role in the biogeochemical cycling of carbon, iron, sulfur, and many trace elements. While a wide range of

oxidation states for Mn is known (-3 to +7), the most common oxidation states found in nature are +2, +3, and +4; with +2 corresponding to the reduced soluble form, and +3 and +4 being the less soluble oxidized forms. The main source of oxidized Mn in the modern oceans is riverine flux with only a minor contribution from glaciers and wind-born dust (Poulton and Raiswell, 2002). Sources for Mn(II), on the other hand, include hydrothermal vents and sedimentary, biologically catalyzed Mn(III, IV) oxide reduction coupled to organic matter oxidation, with the latter being the most important source for dissolved Mn (Burdige, 1993).

Despite its low concentration in the modern oxygenated ocean, dissolved Mn(II) is necessary for carbon fixation and biomass generation in the euphotic zone, thus playing a critical role in photosynthesis (Sunda and Huntsman, 1988). While most biologically utilized Mn is recycled in the surface ocean through repeated uptake by photosynthetic organisms and the release through organic matter degradation by heterotrophic organisms, a fraction will reach the seafloor through incorporation into marine organic aggregates. In addition to biological incorporation, soluble Mn(II) can be removed from the water column through oxidation. In the modern ocean with abundant dissolved O_2, the oxidation of Mn(II) is documented in a wide range of marine settings, facilitated by Mn(II)-oxidizing microorganisms (Sunda and Huntsman, 1988). Although it has only recently been shown that Mn(II)-oxidizing microorganisms may conserve energy from the reaction (Yu and Leadbetter, 2020), many bacteria and fungi are known to mediate Mn(II) oxidation, using molecular oxygen or superoxide without energy conservation (Hansel, 2017; Nealson, 2006; Sunda and Huntsman, 1994, 1988; Tebo et al., 2005). Mn(IV) oxides have the ability to influence the availability of trace elements in the ocean including iron, cobalt, nickel, and zinc, and radionuclides, like thorium and protactinium, by particle scavenging. Mn(IV) oxides, thereby, exercise a strong control on the availability and cycling of many bio-essential and particle-

reactive trace elements in the ocean (Hayes et al., 2015; Jeandel et al., 2015; Means et al., 1978; Murray, 1975; Tonkin et al., 2004; Yamagata and Iwashima, 1963).

Mn(IV) oxide particles sink to the ocean floor, and if oxygen has been consumed by heterotrophic bacteria, Mn(IV) is respired to Mn(II) coupled to organic matter oxidation, a process known as dissimilatory Mn reduction (DMR). While the general view is that the final product of DMR is Mn(II), some studies report the production of soluble or ligand-complexed Mn^{3+} (e.g., (Ehrlich, 1987; Jones et al., 2020). The Mn(II) produced during DMR is released into porewater or an anoxic water column, along with inorganic carbon, or may be organically complexed (Elderfield, 1981). Most of the Mn(II) produced by DMR during diagenesis is transported upward into the overlying oxic sediments, where through the reaction with oxygen, it is converted back into Mn(IV) oxides, with only a minor fraction escaping re-oxidation and reaching bottom waters as aqueous Mn(II) (Sundby, 1977; Thamdrup et al., 1994). It is also likely that some oxidized Mn escapes the sediment. The degree to which Mn(II) is fluxed from the sediment pile into the overlying bottom water depends on the availability of benthic O_2. The diffusive flux of Mn(II) can be enhanced through increased organic matter delivery, a higher export flux of Mn(IV) oxides, or the limited availability of alternative terminal electron acceptors for organic matter oxidation such as nitrate (Burdige, 1993), which leads to increased Mn(IV) oxide reduction.

Unlike the modern oxygenated oceans, where widespread oxidation of Mn limits the concentration of Mn(II) available to the nanomolar (10^{-9} M) range, the pervasively anoxic oceans of the early Earth would have allowed the accumulation of dissolved Mn(II) to tens or even hundreds of micromolar (10^{-6} M). Such conditions are similar to modern anoxic freshwaters, where DMR below the chemocline may result in an appreciable pool of dissolved Mn^{2+}. Notably, Brownie Lake, a modern permanently stratified anoxic iron-rich lake in Minnesota, shows a strong Mn gradient across the redox boundary in the water column with the concentration of dissolved

196 Mn(II) exceeding 100 μM, about five orders of magnitude higher than that observed in modern
197 oxygenated oceans (Lambrecht et al., 2018). Similarly, the anoxic, sulfide-rich water of the Black
198 Sea shows Mn^{2+} concentrations of up to 10 μM, suggesting a wide range for Mn(II) is possible in
199 anoxic settings. While factors such as differences in the flux of Mn particles and rate of Mn(IV)
200 reduction can explain such a wide range of Mn(II) concentrations in modern anoxic settings, the
201 formation of Mn(II) sulfide minerals (e.g., alabandite and rambergite) under the sulfide-rich
202 conditions of the Black Sea could provide a possible explanation that accounts for the lower
203 concentration of Mn(II) in the water column than was observed by Lewis and Landing (1991).
204 Support for such a mechanism can be drawn from reported authigenic Mn(II) sulfide minerals in
205 the Landsort Deep in the Baltic Sea (Lepland and Stevens, 1998). Unlike iron sulfide minerals that
206 are commonly reported and observed in a wide range of modern anoxic settings, the formation of
207 Mn(II) sulfide minerals is less common and appears to occur in environments where the
208 concentration of sulfide is high. For instance, synchrotron-based microprobe techniques on anoxic,
209 sulfide-rich sediments in Fayetteville Green Lake, New York, suggest the presence of Mn(II)
210 sulfide below the chemocline, where the concentration of sulfide reaches up to several mM
211 (Herndon et al., 2018). There is no evidence for significant Mn(II) sulfide formation in the Archean
212 oceans, and pervasively iron-rich and low-sulfate conditions, as indicated by numerous
213 geochemical proxies, suggest a minor, if any, role for Mn(II) sulfide minerals in the Archean
214 marine Mn cycle.

215 Another potentially important sink for reduced Mn(II) under anoxic conditions is the
216 formation of Mn(II) carbonates. While observations from modern anoxic settings suggest that most
217 Mn(II) produced by DMR would diffuse upward and react with oxygen to form Mn(IV) oxides at
218 the oxic-anoxic boundary (Jones et al., 2011), a maximum of Mn(II) may form just below the

boundary due to vigorous Mn(IV) oxide reduction (Herndon et al., 2018). Microbial sulfate reduction at this boundary, which produces bicarbonate via concomitant organic matter oxidation, can lead to supersaturation of pure Mn carbonates (e.g., rhodochrosite, pseudo-kutnahorite) (Jones et al., 2011). These steps are well demonstrated in Lake Matano, Indonesia, where more than 90% of the Mn(II) produced through DMR is re-oxidized, with <10 % exported as solid Mn(II) species (Jones et al., 2011). Manganese(II) carbonates have also been observed in the anoxic, iron-rich Brownie Lake in Minnesota, suggesting that formation may occur at the oxic-anoxic boundary, where the concentration of O_2 is below 5 μM (Wittkop et al., 2020). Specifically, at the chemoclines of both Brownie Lake and Lake Matano, where the concentration of O_2 falls below 5 μM, the high carbonate alkalinity pool, resulting from organic matter breakdown, in combination with elevated Mn(II) from the reduction of Mn(IV), leads to the supersaturation of Mn carbonates. While the generation of small Mn(II) carbonates deposits may be possible, it is important to note that the development of Mn(II) carbonates in these sediments requires the oxidative cycling of Mn(II) to Mn oxides, and subsequent formation of Mn carbonates during diagenesis.

3. Chemical pathways for Mn(II) oxidation

In the modern oceans, the microbially mediated oxidation of Mn(II) by molecular O_2 is the most dominant pathway for the production of Mn(IV) oxides (e.g., Tebo et al., 2005); however, Mn(IV) oxides may be produced without the involvement of O_2 through various abiotic and biotic pathways. While knowledge of potential Mn(II) oxidation pathways is key to models of biogeochemical Mn cycling under various environmental conditions, it is also critical to interpreting the record of Mn deposits that pre-date the rise of oxygen. Prior to the GOE, molecular O_2, the most potent Mn(II) oxidant, was nearly absent in the coupled ocean-atmosphere system,

except for in productive surface waters where O_2 oases were likely present (Olson et al., 2013). In this section, we review the possible biotic and abiotic pathways for Mn(II) oxidation and discuss the viability of each pathway in explaining the pre-GOE Mn records (Fig. 2).

3.1 Biotic oxidation of Mn(II)

Biological oxidation of Mn(II) with O_2 by multi-copper oxidase enzymes in bacteria and related laccase enzymes in fungi has long been recognized despite the lack of energetic benefit to the organisms (Hansel, 2017) (Fig. 2a and b). Recently, a bacterium was shown to conserve energy from O_2-independent chemolithoautotrophic growth by oxidizing Mn(II), with electron transfer possibly mediated through terminal oxidases (Yu and Leadbetter, 2020). Relevant to marine environments is the oxidation of Mn(II) by superoxide, which is produced from O_2 reduction by animal haem peroxidases in bacteria and fungi (Hansel et al., 2012; Learman et al., 2011). Superoxide-mediated Mn oxide formation has recently been demonstrated for phototrophs (Chaput et al., 2019), although superoxide production is also ubiquitous in the deep ocean (Diaz et al., 2013).

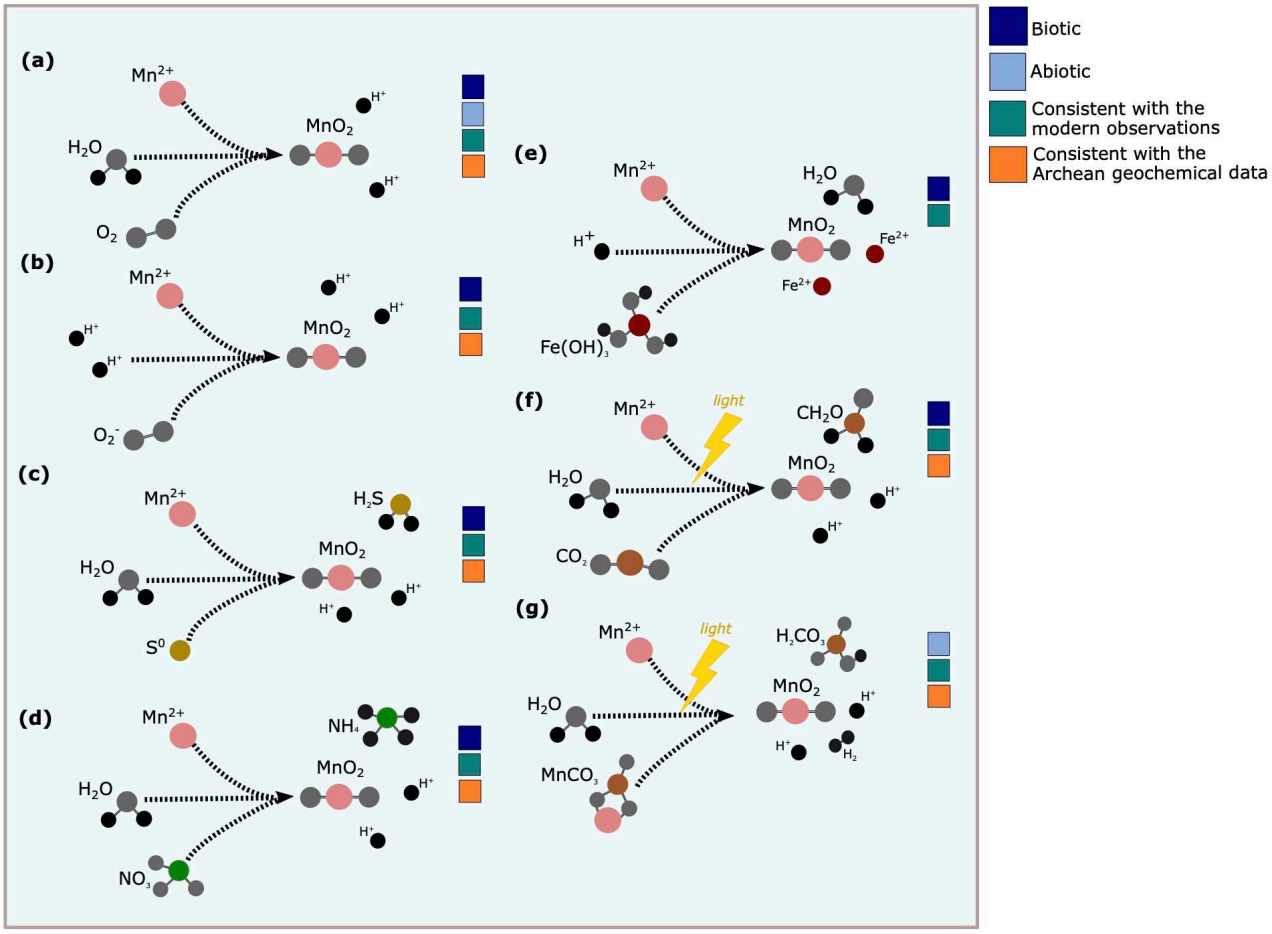

Figure 2. Possible pathways for dissolved manganese (Mn(II)) oxidation include oxidation of manganese by (a) oxygen, (b) superoxide (c) oxidized sulfur (e.g., S^0), (d) nitrate (NO_3), (e) ferric iron (Fe(III)), (f) anoxygenic phototrophy, (g) photooxidation. While there are multiple pathways for the oxidation of Mn(II) in the modern oceans, under Archean, iron-rich conditions, oxidation of manganese is most likely to occur biologically through the presence of molecular oxygen (a) or abiotically through photooxidation of Mn(II) carbonates (e.g., rhodochrosite) (g).

Perhaps the most prominent environmental signal for Mn(II) oxidation with molecular O_2 is the observation of a peak in particulate Mn concentrations at the oxic-anoxic boundary in modern redox-stratified settings (e.g., Jones et al., 2011). This peak is a direct result of the reaction of Mn(II), produced through DMR, that is transferred through molecular or turbulent diffusion to overlying oxygenated waters or porewaters, where it reacts with oxygen and generates a peak in

the Mn-oxide depth profile. While a wide range of organisms facilitate the transformation of Mn(II) to Mn(IV) oxides using O_2, the biochemical and genetic details of this oxidation pathway are yet to be fully resolved.

When O_2 is absent, oxidation of Mn(II) may occur using other oxidants. For instance, by culturing biofilms recovered from a modern anoxic meromictic sulfide-rich lake, a recent study reported the formation of Mn(III, IV) oxides under anoxic conditions (Daye et al., 2019). Alternative oxidants for the formation of Mn(III,IV) oxides under such conditions remain uncertain. However, the absence of conspicuous, thermodynamically feasible oxidants in the culture medium, as well as the known capacity for sulfur metabolism and moderately high-potential photosynthetic reaction centers in the cultured microorganisms (e.g., green sulfur bacterium *Chlorobium sp.*), indirectly suggest the possible involvement of S-species in oxidizing Mn(II) (Fig. 2c). Based on their results, it is possible that Mn(II) oxidation could have been coupled with the reduction of elemental sulfur under anoxic sulfur-rich conditions:

$$CO_2 + 2H_2S + \text{light} \longrightarrow CH_2O + 2S^0_{(s)} + H_2O \quad (1)$$

$$Mn^{2+} + S^0_{(s)} + 2H_2O \longrightarrow MnO_{2(s)} + HS^- + 3H^+ \quad (2)$$

where the first reaction produces elemental sulfur via anoxygenic photosynthesis using hydrogen sulfide as the electron donor (the canonical metabolism of green sulfur bacteria), and the second reaction couples Mn(II) oxidation to elemental sulfur reduction (Van Cappellen et al., 1998; Henkel et al., 2019; Katsev et al., 2004). Such a pathway implies that the anoxic formation of Mn(III, IV) is possible through coupling with sulfide-based anoxygenic photosynthesis. Energetically, the second reaction is only favorable under circumneutral to mildly alkaline pH

conditions and at low concentrations of sulfide. This metabolic pathway would require appreciable sulfide, likely generated through sulfate reduction, to be subsequently oxidized to elemental sulfur. However, at the same time, sulfide concentrations would need to remain below a critical threshold.

To assess the thermodynamic favourability of the formation of Mn oxides by the reaction of Mn(II) and elemental sulfur (reaction 2), we conducted a simple Gibbs Free Energy calculation (ΔG). The value of ΔG was calculated for high (100 μM) and low sulfide conditions (10 μM). To better bracket the range of environmental conditions under which this pathway can be energetically favorable, we employed a stochastic approach in which concentrations of different species were randomly selected from a range of values and the most probable range of ΔG values at different sulfide levels was obtained. The calculation was done for two different Mn oxide minerals of pyrolusite and birnessite. The ranges of Mn(II) and pH were assumed to be between 100 to 500 μM and 6 to 7, respectively, consistent with the suggested range of Mn(II) and pH in the Archean oceans (Halevy and Bachan, 2017; Jones et al., 2011). As shown in Fig. 3, thermodynamic considerations suggest that at sub-mM concentrations of Mn(II), the formation of Mn oxides is only possible if sulfide levels are below 100 μM. This sulfide range (and pH) is consistent with culture-based experiments with green sulfur bacteria and provides an explanation for the apparent anaerobic Mn(II) oxidation (Daye et al., 2019). Notably, there was an absence of Mn(III,IV) oxide mineral production in experiments with 1 μM Mn(II) or 1 mM sulfide (Daye et al., 2019).

Observations from the modern sulfide-rich Black Sea provide further support for interactions between Mn(II) and sulfur cycling under sulfidic conditions. In this case, high concentrations of hydrogen sulfide have been shown to couple with the reduction of Mn oxides, producing oxidized sulfur species (e.g., SO_4, S_2O_3) and Mn(II) (Henkel et al., 2019). This situation differs from the above mechanism where elemental sulfur oxidized Mn(II), as the high sulfide is

316 contributing to the formation of Mn-sulfides following Mn oxide reduction (e.g., Kiratli and Ergin,
317 1996; Herndon et al., 2018).. Results from modern sulfide-rich freshwaters also indicate that
318 oxidation of sulfide by Mn(IV) oxide can result in the production of sulfate and Mn(II), and the
319 sulfate produced through this pathway can be used to oxidize the biologically produced methane
320 in the anoxic water column (Su et al., 2020).

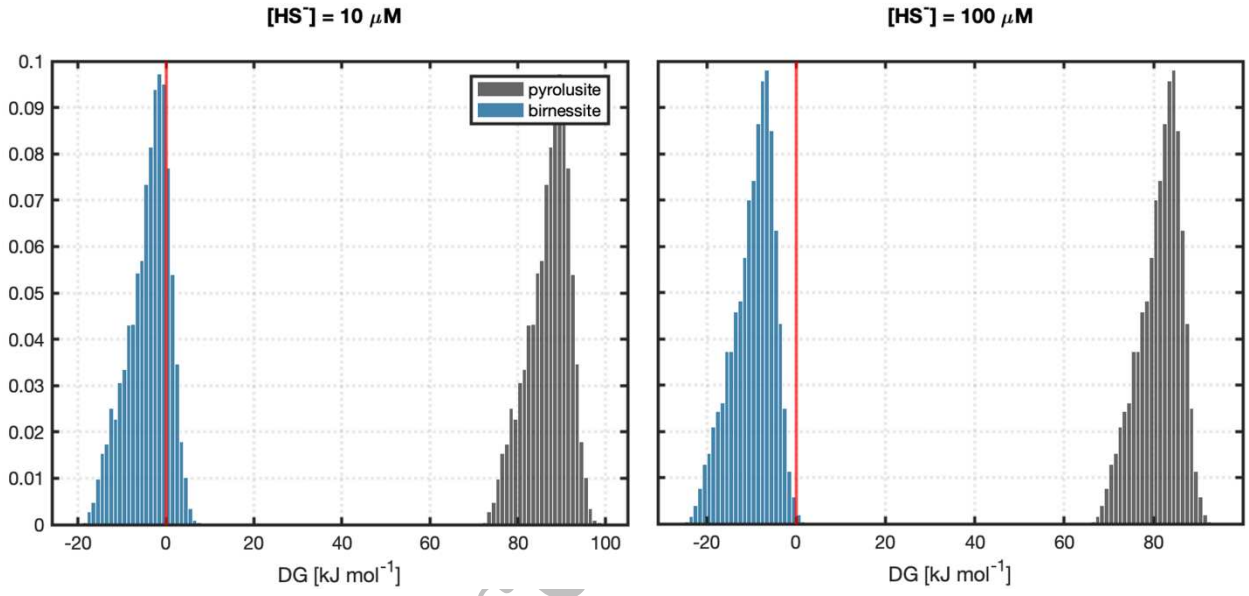

321

322 **Figure 3**. Gibbs-free energy estimation for the favourability of the sulfur-dependent Mn oxidation
323 pathways at two different sulfide concentrations in seawater. Our estimation indicates that sulfur-
324 dependent Mn oxidation is only favorable when seawater sulfide concentration is below 100 μM.
325

326 Another possible biologically mediated pathway to produce Mn oxides is through
327 anoxygenic photosynthesis (non-O_2-producing photosynthesis) (Fig. 2f). Like ferrous iron (Fe^{2+}),
328 anoxygenic phototrophs can theoretically oxidize Mn(II) while reducing CO_2 to biomass (Fischer
329 et al., 2015; Olson, 1970). The formation of Fe(III) (oxyhydr)oxides by anoxygenic photosynthesis
330 is well documented in the modern, anoxic, ferruginous freshwater systems, with implications for
331 the formation of iron formations in the late Archean and Paleoproterozoic (Crowe et al., 2008;
332 Ehrenreich and Widdel, 1994; Swanner et al., 2020). In contrast, the significance of

photosynthetically mediated Mn(II) oxidation in modern settings remains unknown. However, recent observations from optical (UV-visible) and X-ray absorption spectroscopy have shown that through photosystem II (PSII) the light-dependent oxidation of Mn(II) can lead to the formation of a birnessite-type Mn(III, IV) oxide, providing experimental support for the possibility of ancient Mn oxidation photosystems (Chernev et al., 2020). Yet, despite these recent efforts to identify a microbe capable of photosynthetic Mn^{2+} oxidation, this metabolism has not yet been demonstrated in an extant microbial lineage.

Other potential electron acceptors for the oxidation of Mn(II) under anoxic conditions are iron oxides (e.g., $Fe(OH)_3$) and nitrate (NO_3) (Fig. 2d & 2e). The possible pathway for Mn(II) oxidation using Fe(III) is described by (Davison, 1993):

$$2\,Fe(OH)_3(s) + Mn^{2+} + 2\,H^+ \longrightarrow 2\,Fe^{2+} + MnO_2(s) + 4\,H_2O. \quad (3)$$

This pathway may be thermodynamically feasible under mildly acidic conditions, where the concentration of dissolved ambient iron is extremely low. However, the potential for Mn oxidation with iron oxides as the electron acceptor under anoxic conditions in natural systems remains poorly constrained. Conversely, the reverse reaction – the oxidation of dissolved Fe^{2+} with MnO_2 – is possible, and well-known, under a wide range of environmental conditions (Davison, 1993; Schaefer et al., 2017). This reverse reaction is likely to be quantitatively more important and plays a critical role in separating Mn and Fe in aqueous systems. The importance of the reverse reaction is supported by observations in the geological record such as in the Sinqeni Formation (Smith and Beukes, 2023) and the Hotazel Formation (see Fig. 2 in Gutzmer and Beukes, 1995), where Mn

355 enrichment only occurs once Fe becomes depleted, implying that any remaining Fe^{2+} reacts with
356 any formed $Mn^{3+/4+}$, keeping it in solution until the Fe is mostly removed.

357 Nitrate is another thermodynamically feasible electron acceptor for the oxidation of Mn(II).
358 Evidence for NO_3^--driven oxidation of Mn(II) is scarce in modern aqueous systems, but it may
359 occur through the following pathways:

360

361 $$4\ Mn^{2+} + NO_3^- + 5\ H_2O \longrightarrow 4\ MnO_{2(s)} + NH_4^+ + 6\ H^+ \quad (4)$$

362

363 $$4\ Mn^{2+} + NO_3^- + 5\ H_2O \longrightarrow NH_3 + 4\ MnO_{2(s)} + 7\ H^+ . \quad (5)$$

364

365 Apparent evidence for Mn(II) oxidation with nitrate as the electron acceptor can be found from the
366 observation of Mn(IV) oxide production in sediments in which O_2 is nearly absent and there is no
367 apparent spatial overlap between Mn(II) and O_2 in 1D depth profiles, with nitrate being the only
368 other abundant oxidant for dissolved Mn(II) in that region of the sediment column (Boudreau et
369 al., 1998; Jung et al., 2017; Luff and Moll, 2004). Thermodynamically, this reaction is only
370 favorable under relatively alkaline conditions and with a high concentration of NO_3^-. Based on
371 incubation experiments under anoxic conditions, the reduction of MnO_2 increased NO_3^- production
372 when the MnO_2 level is high (Hulth et al., 1999). Direct tests, however, provided no evidence for
373 Mn-dependent NH_4^+ oxidation, even in Mn oxide-rich sediments or with exogenous Mn(III)
374 (Crowe et al., 2012).

375

376 *3.2 Abiotic oxidation of Mn(II)*

Production of Mn(III/IV) oxides can occur without biological involvement, although rates of abiotic oxidation reactions tend to be much slower than those characteristic of biotic pathways. The biotic oxidation of Mn by molecular O_2 is reported to be many times more rapid than the abiotic pathway (e.g., Diem and Stumm, 1984), although there is a strong pH dependence below pH 9. The sluggish kinetics of abiotic oxidation of Mn(II) can be offset by organic and inorganic catalysts, as well as reactive oxygen species. Specifically, the abiotic oxidation of Mn(II) can potentially be catalyzed by molecular O_2 or through complexation with organic compounds (e.g., ligands) (Nico et al., 2002; Duckworth and Sposito, 2005) or by Mn oxide mineral surfaces (Diem and Stumm, 1984; Davies and Morgan, 1989; Junta and Hochella, 1994). For instance, experimental studies show the possibility of abiotic oxidation of Mn(II) to amorphous Mn(III, IV) on the surface of magnetite (Fe_3O_4) and hematite (Fe_2O_3) (Ren et al. 2013). Experimental studies suggest that abiotic oxidation of Mn(II) that involves mineral surfaces can be kinetically competitive relative to the biologically-mediated oxidation of Mn(II) (e.g., Ren et al. 2013). Reactive oxygen species, on the other hand, can have both positive and negative impacts on the oxidation rate of Mn(II). For instance, superoxide (O_2^-) can result in an enhancement in the abiotic oxidation of Mn(II) while hydrogen peroxide (H_2O_2) can act as a reductant for Mn oxides (Godwin et al. 2020).

Light is another important catalyst for the abiotic oxidation of Mn(II) (Anbar and Holland, 1992; Jung et al. 2017; Liu et al., 2020) (Fig. 2g). For instance, experimental studies suggest that in the presence of light, oxidation of Mn(II) to Mn(IV) catalyzed by the superoxide radical, generated from photolysis of nitrate, can have rather fast kinetics (Jung et al. 2017). This photochemical pathway results in the formation of birnessite (Jung et al. 2017). Light energy available in the photic zone of the ocean can oxidize Mn(II) without requiring oxidants such as O_2

400 and elemental sulfur or high-potential photosynthetic reaction centers (Liu et al., 2020). The idea
401 of Mn(II) and Fe(II) photooxidation is not new (Cairns-Smith, 1978), and recent experimental
402 findings indicate that the abiotic photooxidation of rhodochrosite ($MnCO_3$) under anoxic
403 conditions can produce manganite (Mn(III)OOH) and H_2 gas (Liu et al., 2020). Similarly, Mn(II)
404 can be oxidized through photocatalytic reactions with superoxide radicals produced by the
405 photolysis of nitrate (Jung et al., 2017) or on the surfaces of iron and titanium oxides (Jung et al.,
406 2021b, 2021a). The overall pathway for such photooxidation is:
407
408 $$2Mn(II)CO_3 + 4H_2O \xrightarrow{h\nu} 2Mn(III)OOH + H_2 + 2HCO_3^- + 2H^+ \quad (6)$$
409
410 The reaction described by Liu et al. (2020) is the proposed mechanism most relevant to the
411 early oceans and proceeds at an incident wavelength of around 230 nm. This suggests a possible
412 role for this pathway in forming Mn oxides in very shallow-water environments since the light in
413 such UV wavelengths is strongly attenuated with depth. The plausibility of this mechanism,
414 however, is low as rhodochrosite would not likely have accumulated to sufficiently high
415 concentration in the photic zone of the Archean ocean (Lyons et al., 2020). Furthermore, complex
416 solution chemistries that are closer in salinity to that of seawater have been shown to inhibit
417 photooxidation of Fe^{2+} (e.g., Konhauser et al., 2007), suggesting that to some degree shielding by
418 the water column may prevent widespread UV photooxidation of reduced, aqueous species.
419
420 *3.3 Insights into possible Mn(II) oxidation pathways on the Archean Earth: A synthesis*
421 Despite a wide range of possibilities for the oxidation of Mn(II) in modern oxic and anoxic settings,
422 there are only a few biotic pathways for Mn(II) oxidation that are relevant for Archean oceans

because low concentrations of Mn(II) oxidants and high concentrations of labile Mn reductants (like Fe^{2+}) would have limited Mn(II) oxidation in the absence of O_2. Assuming no O_2 involvement in the production of Archean Mn(II) oxides, the next available oxidants under anoxic conditions would have been oxidized sulfur (e.g., elemental sulfur), nitrate, and iron oxides. However, all these remain, at best, poorly supported as important Mn oxidants based on observations in modern environments and would likely have been of minor abundance in the 3.0 billion-year-old oceans. The sulfur-dependent oxidation of Mn(II), as discussed above, would likely require a high concentration of elemental sulfur. Under extremely low-sulfate conditions of the Archean oceans (Crowe et al., 2014; Habicht et al., 2002; Halevy, 2013), biologically mediated formation of elemental sulfur was likley insignificant; however, photochemical production of elemental sulfur in the atmosphere could have been an important source of the elemental sulfur to the oceans. It is nevertheless unclear if the flux of photochemically produced elemental sulfur to the surface ocean would have been large enough to result in pervasive oxidation of Mn(II), implying a limited role for elemental sulfur in the formation of Mn oxides. To this end, we note that pre-GOE sedimentary Mn-enrichments are generally lacking in sulphide minerals (Smith and Beukes, 2023; Smith et al., 2023), which would be expected to form as a byproduct of the oxidation of Mn^{2+} by elemental S through the concomitant generation of reduced sulphur (see reaction 2).

Archean nitrogen isotope records suggest an insignificant role of nitrate in the global nitrogen cycle before the GOE, implying an unimportant role, if any, in facilitating Mn(II) oxidation in anoxic waters (Mettam et al., 2019; Zerkle et al., 2017; Zerkle and Mikhail, 2017). We note that for a 2.9 Ga granular iron formation, nitrate within the water column was viewed as a potentially important oxidant for organic carbon (Smith et al., 2017). Perhaps more importantly, however, by 2.5 Ga there is evidence for the accumulation of nitrate in local environments within

446 the Mt. McRae shale in western Australia and the Campbellrand-Malmani platform from South
447 Africa (e.g., Garvin et al., 2009; Godfrey and Falkowski, 2009; Busigny et al., 2013). Under
448 Archean ferruginous (Fe(II)-rich) conditions, the accumulation of Mn oxide through iron oxide
449 reduction was also unlikely, even if iron oxides were being widely produced through
450 photoferrotrophy, because preservation of Mn oxides would be hampered by the ambient Fe(II) in
451 the Archean ocean (i.e., reversed reaction 3 that leads to the separation of Mn and Fe in aqueous
452 systems) (Jones et al., 2011) (more on this below).

453 By analogy to the O_2-replete modern ocean, the most likely pathway for quantitatively
454 important Archean Mn(II) oxidation would have been via molecular O_2 or superoxide produced
455 through photosynthesis in the surface ocean. These oxidants would have reacted with available
456 Mn(II) transported from anoxic deep waters in a manner similar to that observed in modern anoxic
457 waters and sediments (Jones et al., 2011). Any operation of this pathway during the Archean
458 implies the rise of oxygenic photosynthesis and at least local O_2 accumulation before the rise of
459 atmospheric oxygen associated with the GOE. This possibly is consistent with Archean
460 geochemical proxy records including fractionated Cr and Mo isotopes at roughly three billion years
461 ago (Crowe et al., 2013; Planavsky et al., 2014).

462 Archean Mn oxides could have been produced abiotically through photooxidation. There
463 are two main factors to consider with respect to the occurrence and importance of Mn(II)
464 photooxidation (Liu et al., 2020) under Archean conditions: light intensity and the presence of
465 rhodochrosite ($MnCO_3$). Photons of the required wavelengths (~230 nm) for extensive Mn(II)
466 photooxidation were likely for the Archean oceans and continents, although solar luminosity was
467 at about 80% of its modern value and so the light intensity incident to the outer atmosphere would
468 have been weaker. We note, however, that radiation incident to the surface oceans would also have

depended on atmospheric composition. Results from modern permanently stratified freshwater systems, as the best analogs for the chemistry of Archean oceans, point to the possibility of appreciable rhodochrosite ($MnCO_3$) formation in anoxic waters (Herndon et al., 2018; Wittkop et al., 2020). As noted above, the reduction of Mn oxides in the water column could have led to elevated dissolved Mn(II) and localized $MnCO_3$ supersaturation. Importantly, photooxidation of Mn(II) in rhodochrosite results in the production of H_2, and the H_2 released through this process could have fueled ancient microbial metabolisms and aided in Earth's surface oxygenation through hydrogen escape (Liu et al., 2020). However, two key questions remain concerning the potential role of Mn photooxidation: (i) its potential quantitative importance and (ii) the efficiency of this reaction at higher, marine salinities. Specifically, it has been questioned whether rhodochrosite would have accumulated to appreciable concentrations in the photic zone of the Archean ocean, as precipitates should have settled through the water column quickly (Lyons et al., 2020). Further, experimental work on the photooxidation of Fe by UV light has shown that photooxidation becomes negligible under solution chemistries like those expected for the Archean ocean (Konhauser et al., 2007). Notably, Mn photooxidation has only been demonstrated under relatively simple solution chemistry (Liu et al., 2020), and it remains to be seen whether this process could have occurred under conditions more representative of the Archean oceans.

4. Preservation of Mn oxides during the Archean

Regardless of the possible biotic and abiotic pathways for the production of Mn(III, IV) oxides, preservation of Mn oxides in the sedimentary rock record (delivery to the seafloor and subsequent burial) likely required a lack of Mn reductants in overlying waters. In anoxic, iron-rich Archean oceans, the reduction of Mn oxides coupled with the oxidation of organic matter and Fe^{2+} would

492 likely have caused the dissolution of the Mn oxides before they reached the seafloor. Once on the
493 seafloor, organic matter oxidation proceeds through a cascade of electron acceptors according to
494 their availability and free energy yields (Froelich et al., 1979). For the preservation of Mn oxides,
495 conditions within the sediment pile would have required that O_2 or nitrate act as the primary
496 terminal electron acceptors during organic matter oxidation, both of which require O_2. Comparing
497 the timescale for Mn oxide export from the water column to the kinetics of the reactions for
498 organic- and Fe-driven Mn reduction can offer some insights into the extent of Mn oxide
499 preservation under ferruginous Archean conditions. An important implication for
500 paleoenvironmental interpretations is that even if Mn(IV) oxides are formed in the absence of O_2
501 through abiotic pathways, their delivery to the sediments would almost certainly necessitate O_2
502 within the water column in order to achieve export to the seafloor.

503 To provide an estimate of the Mn oxide preservation potential, we consider a simple
504 calculation to estimate the settling time through the Archean ocean water column. We
505 conservatively assume the settling velocity of Mn(IV) oxide particles to be on the order of 10 m
506 d^{-1} (which is more than twice what is observed in the modern anoxic, iron-rich lakes (e.g., Jones
507 et al., 2011) and depth to be around 100 meters, typical for the surface mixed-layer in the modern
508 oceans. This leads to a settling rate for Mn oxides through a 100 m Achaean ocean water column
509 that would have been on the order of 0.1 d^{-1}. Effective preservation of Mn oxides would only occur
510 if the deposition rate would outcompete the destruction rate of Mn(IV) oxide through the reduction
511 of Mn oxides by organic matter and Fe(II) oxidation. Reported rate constants for Mn reduction
512 with organic matter are between 1 to 5 d^{-1} (e.g., Jones et al., 2011; Stumm and Morgan, 1996).
513 These values are about an order of magnitude higher than the rate constant for the deposition of
514 Mn oxides, suggesting that Mn oxides would have been reduced in an anoxic water column prior

to burial in the sediment. Considering a depth of 10 meters for the water column, the deposition rate can be comparable to the reduction of Mn oxides by organic matter, implying that some Mn oxides may escape reduction and reach the seafloor, at depths less than 10 meters. This simple calculation, however, does not account for the reduction of Mn by Fe(II). Assuming a conservative estimate for Archean seawater Fe(II) concentration on the order of 10 μM (Konhauser et al., 2017), the rate constant of Mn reduction by Fe(II) would be on the order of 10 d^{-1} (Van Cappellen and Wang, 1996), which suggests that Mn reduction would outpace Mn oxide deposition in a water column with a depth of 10 m under anoxic and ferruginous conditions.

Observations from modern ferruginous lakes provide further insight into the potential for the preservation of Mn oxides under anoxic conditions similar to those of Archean oceans. For example, in Lake Matano, Indonesia, an almost complete reduction of Mn oxides in the water column was observed (Jones et al., 2011). Results from synchrotron-based X-ray fluorescence and X-ray spectroscopic analyses of bottom sediments and sinking particles in Lake Matano indicate a highly efficient reduction of Mn oxide under anoxic conditions, with almost no Mn oxide export to sediments underlying anoxic waters (Jones et al., 2011). These observations further indicate that the depth of Mn oxide penetration into anoxic waters is less than 2 meters, and below this depth, the oxides are reduced via oxidation of organic matter, Fe(II), H_2S, and possibly CH_4 (Jones et al., 2011). While the presence of sulfide may limit the relevance to the Archean, the ancient oceans were replete in Fe(II) whose oxidation in shallow waters would have led to enhanced Mn oxide reduction. Notably, the penetration depth depends on the settling velocity of Mn oxide particles as well as reductant concentrations. Fe(II) concentrations are expected to have been similar in the Archean oceans (Crowe et al., 2008). Further, Mn oxide settling velocities would have depended on particle size and density, as well as the extent of aggregation. In the absence of information on

settling velocities in the Archean oceans, we assume that they were similar to those in modern Lake Matano. Manganese oxide penetration depths may thus have been similar in the Archean oceans, implying that under anoxic ferruginous conditions, Mn oxides would only be preserved in extremely shallow waters. This interpretation is inconsistent with suggestions of Mn oxide deposition and enrichments in sediments below wave base (>150 meters; Boggs, 1995) in the Archean-Paleoproterozoic rock record (Ostrander et al., 2019), suggesting the importance of some O_2-containing surface waters.

For instance, Mn-rich carbonates of the Hotazel Formation offer strong evidence for the diagenetic reduction of an Mn(III, IV) precursor within the sediment pile, and these were deposited below the wave base. Taken together, the above approximation of Mn oxide settling, along with the observations from the modern ferruginous lakes, suggests that while traces of Mn oxide might be potentially produced in the absence of environmental O_2, their export to sediments and preservation requires sufficiently oxidizing conditions and O_2 in order to limit the accumulation of Fe(II), which would reduce Mn oxides. The presence of O_2 would also preclude water column Mn oxide reduction by organic matter, which happens only under very low O_2 levels or anoxia. We note that in extreme cases, where sediment accumulation is very rapid, Mn oxides may be buried before they are reduced, which may complicate diagenetic pathways. Given the free energy yields of possible terminal electron acceptors, the accumulation of O_2 or nitrate, which itself requires O_2, would be required to consume organic matter and limit the reductive dissolution of Mn oxides.

The inferred preservation of Mn oxides all the way to the seafloor and isotopically light carbon in Mn-carbonates assumed to form during diagenesis thus likely required deposition from a Fe(II)-free, at least mildly oxygenated Archean water column. Collectively, these arguments

yield some of our earliest geochemical evidence for O_2 accumulation in the surface ocean (Planavsky et al., 2014; Ossa Ossa et al., 2019) and thus the early occurrence of biological O_2 production during photosynthesis.

While the organic matter is generally viewed as leading to the reduction of Mn(IV) through DMR, it is also possible that some degree of association of Mn with the organic matter may insulate Mn oxides from reduction. For example, organic complexes may stabilize Mn(III) in porewaters, accounting for an appreciable fraction of the dissolved Mn pool (Madison et al., 2013). The majority of this Mn(III) is generated by the oxidation of Mn(II) by O_2 when upwardly diffusing Mn(II) reaches oxic porewaters; however, a small amount of this Mn(III) may also be attributed to Mn(IV) reduction (Madison et al., 2013). Similarly, organic matter coatings have been shown to insulate Fe(III) oxyhydroxides from reductive dissolution during diagenesis over prolonged timescales (e.g., Lalonde et al., 2012). Whether or not a similar mechanism could also stabilize Mn(III,IV) oxides remains an open question worth exploring given the similarities in the chemistry of Fe and Mn, however such relationships do not seem to enhance Mn oxide preservation in modern settings.

5. Mn oxides in the rock record

The distribution of manganese oxides has been variously used in efforts to reconstruct Earth's redox state (Fig. 4), both through temporal changes in their abundance and their relationships to other geochemical proxies. Often, the temporal trend in sedimentary Mn deposits is juxtaposed against the banded iron formation (BIF) record (Bekker et al., 2014; Maynard, 2010). While the record of Mn ores through time is in many ways decoupled from that of BIF, principally by the presence of Mn ore deposits in the Phanerozoic, there are instances where a clear positive

relationship between Mn and Fe abundances is preserved, such as in the Sinqeni, Koegas, and Hotazel formations in South Africa (Smith, 2018). The decoupling of the Mn ores and BIFs, however, is not purely secular. For instance, Bekker et al. (2003) noted that Mn deposits developed following the Lomagundi excursion, but not BIFs. In part, the decoupling may be ascribed to the differential redox potentials of Fe and Mn, which is reflected in oxidation of Fe(II) prior to Mn(II) (Krauskopf, 1957) and the limited preservation potential for Mn oxides in the presence of Fe(II) as discussed above. Unlike for iron formations where the Phanerozoic record is principally ironstones, there are a number of large Phanerozoic Mn deposits (Fig. 4C). Moreover, the cessation of BIF deposition has been variously attributed to oxygenation, waning iron fluxes to the ocean, and/or the increasing importance of sulfide in the Proterozoic oceans (Bekker et al., 2014; Canfield, 1998; Holland, 1984; Konhauser et al., 2017). It has also been pointed out that large Mn ore deposits are both stratigraphically and geographically constrained relative to the widespread BIFs of the Archean and Paleoproterozoic (Maynard, 2010).

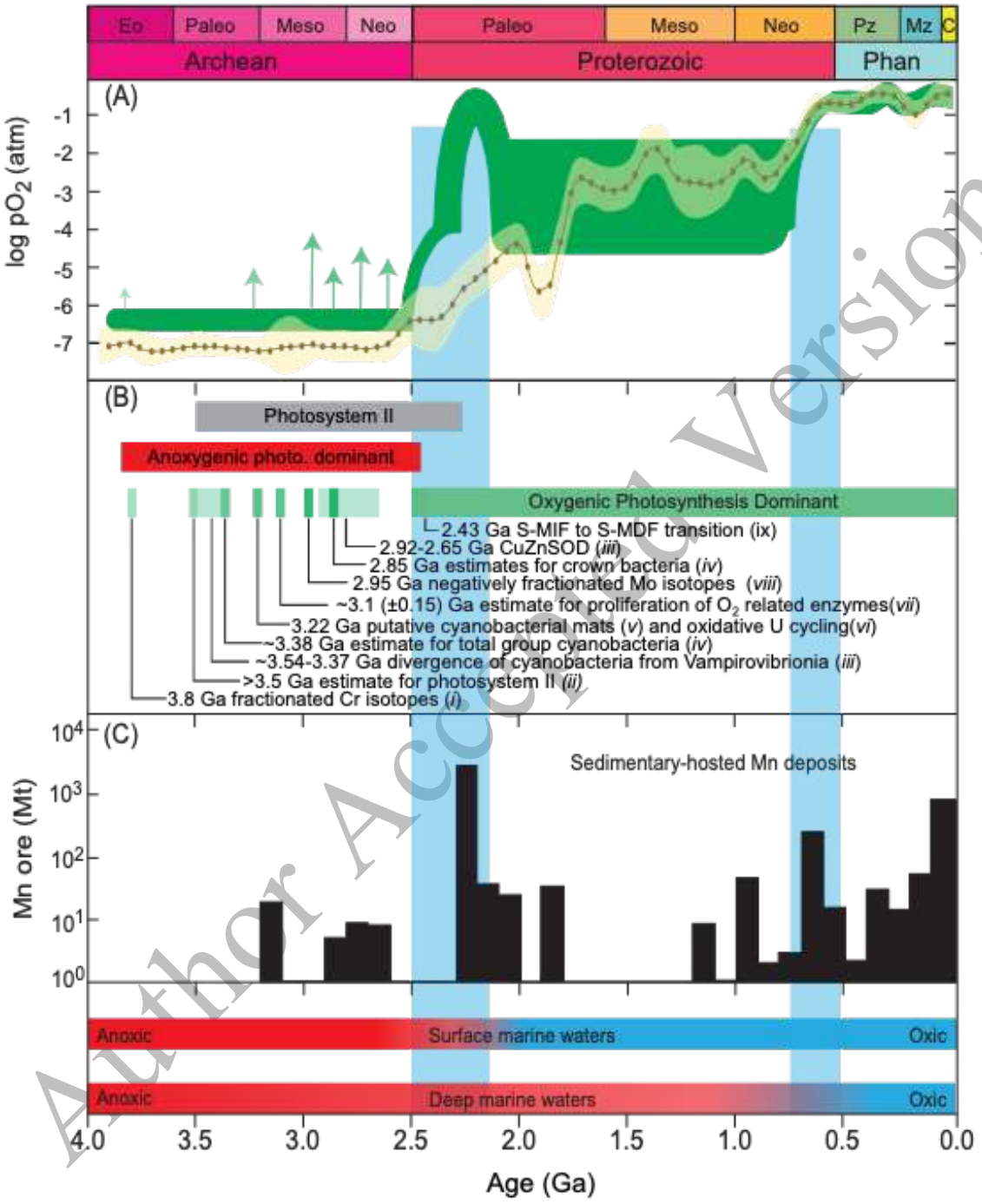

597

598 **Figure 4.** (A) Models for the trajectory of oxygenation of Earth's surface environments from the
599 Archean through to the modern, adapted from Lyons et al., (2014) (green) and G. Chen et al.,
600 (2022) (yellow), including 'whiffs of oxygen' dating back to 3.8 Ga. (B) Age constraints on the
601 evolution of oxygenic photosynthesis, the appearance of photosystem II, and the dominance of
602 anoxygenic photosynthesis from (i) Frei et al., (2016); (ii) Cardona et al., (2018); (iii) Boden et al.,
603 (2021); (iv) Fournier et al., (2021); (v) Homann (2019), (vi) Satkoski et al., (2015); (vii) Jabłońska
604 and Tawfik (2021); (viii) Planavsky et al., (2014); and (ix) Warke et al., (2020) and Bekker et al.,
605 (2020, 2021). (C) The distribution of sedimentary Mn deposits through time adapted from
606 (Maynard, 2010). (D) The redox state of shallow- and deep-marine waters after Alcott et al.,
607 (2019).
608

609 Given both the continued formation of Mn deposits into the Phanerozoic and changes in the tempo
610 and locus of BIF deposition following the GOE, including a general decline in BIF deposition
611 from the Paleoproterozoic to Mesoproterozoic, it was argued that the progressive oxygenation of
612 Earth's surface environments did not exert a strong control on the abundance or distribution of Mn
613 deposits through time (Maynard, 2010). However, it should be noted that the early Proterozoic Mn
614 reserves in the Kalahari Mn Field, South Africa, are by far the largest (Beukes et al., 2016), they
615 thus represent a massive Mn depositional event associated with the GOE.

616 Before examining the linkages between Mn formations and O_2 (Fig. 4), we briefly
617 examine the temporal relationship of South African Mn enrichments leading up to the GOE. The
618 Neoarchean to Paleoproterozoic Transvaal Supergroup of South Africa is preserved in three sub-
619 basins — the Griqualand West, Transvaal, and Kanye — and displays a succession spanning the
620 GOE (Eriksson et al., 2006; Smith and Beukes, 2016). The Griqualand West sub-basin contains
621 the Campbellrand Subgroup, a thick succession of dolomitic carbonates overlain by several
622 hundred meters of BIF of the Kuruman and Griquatown formations of the Asbesheuwels Subgroup
623 (Beukes, 1984). Volcanic ash beds below the Kuruman iron formation yield U-Pb dates of 2521 ±

3 Ma (Sumner and Bowring, 1996), consistent with a maximum depositional age of 2460 ± 5 Ma for the Kuruman Formation (Pickard, 2003). New high-precision U-Pb ages generated for the Kuruman Formation through chemical-abrasion isotope-dilution thermal ionization mass spectrometry (CA-ID-TIMS) place the base of the Kuruman Formation at 2484.6±0.34 Ma and the top at 2464.0 ± 1.3 Ma (Lantink et al., 2019). Overlying the Asbesheuwels Subgroup is the Koegas Subgroup, which, in turn, is overlain by the Makganyene glacial diamictites and the volcanics of the Ongeluk Formation (Tsikos and Moore, 1997). Overlying the Ongeluk Formation is the Hotazel Formation, which hosts the extensive Kalahari Manganese Field (Gutzmer and Beukes, 1995; Tsikos et al., 2010), and is overlain by the Mooidraai Formation (Gutzmer and Beukes, 1995; Kunzmann et al., 2014; Tsikos et al., 2010). Initial U-Pb age estimates place the Ongeluk Formation at 2222 ± 13 Ma (Cornell et al., 1996), while Mooidraai Formation carbonates yield Pb-Pb and U-Pb dates of 2394 ± 26 and 2392 ± 13 Ma, respectively (Bau et al., 1999; Fairey et al., 2013). Recent Re-Os dating of the Nelani Formation of the Koegas Subgroup yields a depositional age of 2479 ± 22 Ma (Kendall et al., 2013), and U-Pb dating of Ongeluk Formation volcanics yields an age of 2426 ± 3 Ma (Gumsley et al., 2017). The importance of understanding the age of these deposits and their relation to the oxygenation of the Achaean to Paleoproterozoic atmosphere and Earth systems evolution is underscored by recent efforts to correlate the Kaapval craton with their equivalents in the Pilbara Craton of Western Australia (see Bekker et al., 2020, 2021; although see Phillipot et al., 2020, for discussion).

The Koegas Subgroup, similar to the Hotazel Formation, contains Mn-enriched intervals (Schröder et al., 2011). X-ray absorption spectroscopy reveals that Mn enrichments are generally restricted to iron formations and concentrated in Mn-bearing carbonates displaying diagenetic textures (Johnson et al., 2013). Schröder et al. (2011) determined that the terrigenous mudstone

and iron formation facies contain Mn concentrations ranging from 0.1 to 11.6 wt% and 0.3 to 16.6 wt%, respectively.

While it has been suggested that the progressive oxygenation of Earth's surface environments may not strongly control Mn deposition, there are still intriguing parallels between the temporal trends in the Mn oxide and BIF records, most notably a peak in the abundance of Mn deposited at 2.4-2.0 Ga (Fig. 4C), which is dominated by the Kalahari Manganese Field of South Africa, and the general absence of Mesoproterozoic Mn deposits. Although we note the recent documentation of two pulses of Mn deposition at ~1.45 Ga and 1.11 Ga recorded in the Ullawarra Formation and Collier and Manganese groups in Western Australia, respectively, that coincide with hypothesized periods of oxygenation in the Mesoproterozoic (Spinks et al., 2023). The Kalahari Manganese Field represents a substantial reserve of Mn, with approximately 8 billion tons with Mn contents varying between 20-48% (Gutzmer and Beukes, 1996, 1995; Tsikos et al., 2003). The extensive Kalahari Manganese Field is hosted in the Hotazel Formation, which also contains several intervals of BIF and has levels of both high-grade Mn oxides and low-grade Mn ores characterized by the presence of braunite (Mn(III) silicate), as well as Mn carbonates (Fig. 5). The depleted $\delta^{13}C$ values for these carbonates suggest oxidation of organic carbon during carbonate formation (Tsikos et al., 2003). In hydrothermally altered high-grade ores, a wider array of Mn oxides is observable. Previously, the Kalahari Manganese Field was dated to about ~2.22 Ga and assumed to coincide with the GOE (Bau and Alexander, 2006). An updated Paleoproterozoic geochronology of the Kaapval craton has demonstrated that the Hotazel Formation, and by extension the Kalahari Manganese Field, is much closer to 2.4 Ga in age (Gumsley et al., 2017).This raises the significant likelihood that the Mn enrichments in the Koegas

669 Subgroup and the Kalahari Manganese Field are in some manner related specifically to the early
670 onset of the GOE that likely extended over hundreds of millions of years (Poulton et al., 2021).

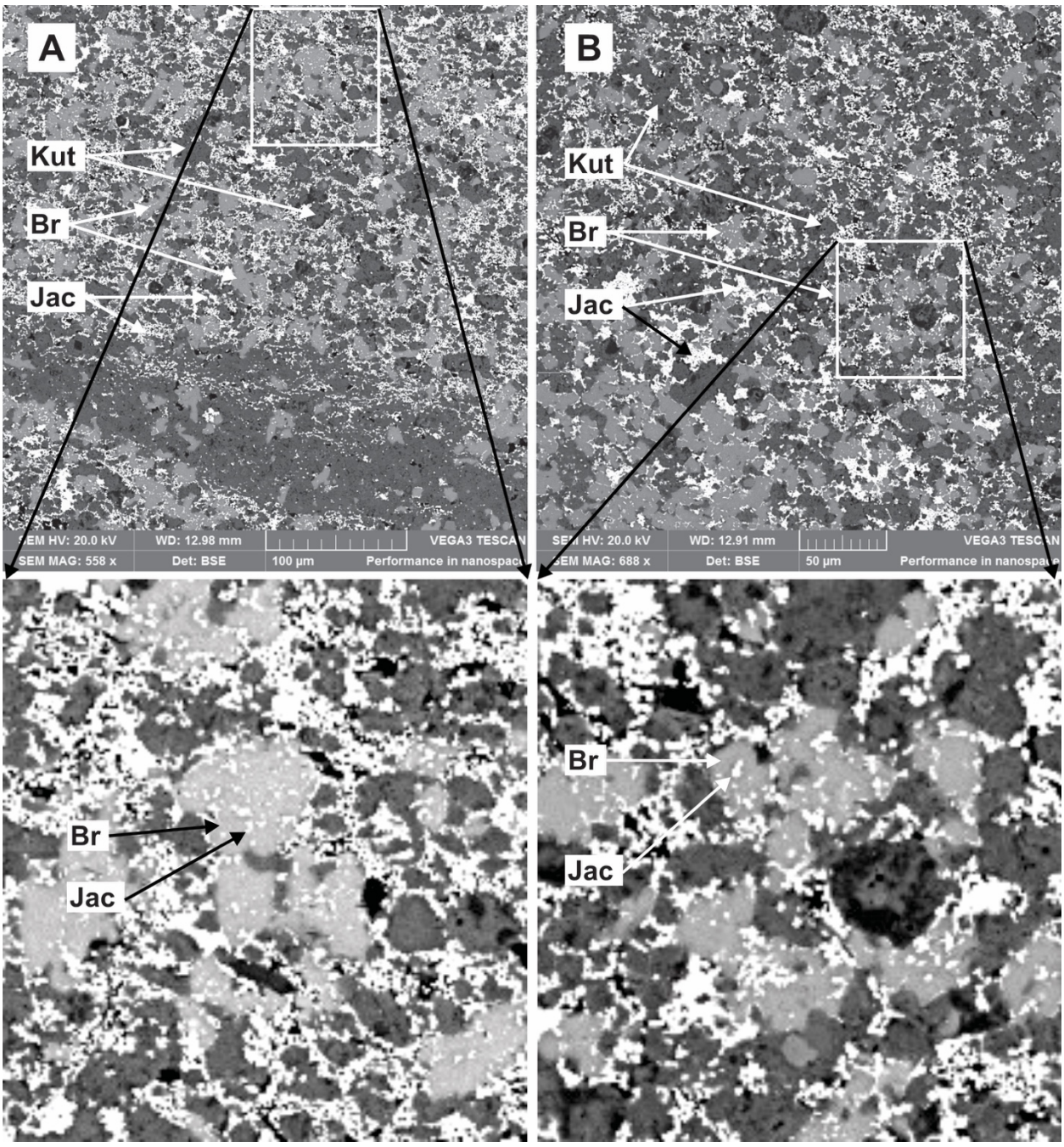

671

672 **Figure 5.** Backscatter electron image under scanning electron microscope showing manganese
673 mineral occurrences in the lower (A) and upper (B) Mn intervals of the ~2.4 Ga Hotazel Formation,
674 Transvaal Supergroup, South Africa. It appears that jacobsite (Jac; $(Mn,Mg)Fe_2O_4$) is the earliest
675 phase as it is overgrown by or included in by braunite (Br; $Mn^{2+}Mn^{3+}{}_6(SiO_4)O_8$). Similarly,

kutnohorite (Kut; $CaMn^{2+}(CO_3)_2$) is interstitial to or overgrows the braunite. Given the close associations, these diagenetic mineral phases with reduced to mixed valence Mn, likely grew in close succession to one another if not near contemporaneously. Samples were collected from a core drilled on the Middelplaats farm, in the south-central Main Kalahari Deposit of the Kalahari Manganese Field. Photo credit: Dillan Fitton.

As noted above, the Hotazel Formation in South Africa is one of the world's largest Mn deposits and has been canonically linked to the onset of the Great Oxidation Event (GOE). As such, the linkages between the Hotazel Formation and the rise of oxygen, require further consideration. As detailed above recent geochronology constraints that have improved our knowledge of the Hotazel Formation's age include Re-Os dating of shales in the Koegas Subgroup (Kendall et al., 2013), and U-Pb dating of Ongeluk Formation volcanics (Gumsley et al., 2017), placing its deposition close to 2.4 Ga deposition shortly after the onset of the GOE.

The Hotazel Formation represents the youngest episode of iron formation deposition in the Transvaal Supergroup and contains extensive Mn deposits. Borehole data has revealed four units of BIF interlayered with three Mn layers consisting of braunite and Mn carbonates (Tsikos and Moore, 1997). To date, the braunite in the Hotazel Formation is the oldest occurrence of preserved oxidized Mn in the rock record. Older successions are characterized by Mn carbonates, which may reflect the effects of Mn reduction. The lower beds of the Hotazel Formation are characterized by oxide-dominated facies, whereas the middle and upper facies are dominated by silicate and carbonate minerals (Tsikos and Moore, 1997). Negative Ce anomalies, indicative of oxygenic conditions, have been documented in the lower Mn-rich beds of the Hotazel Formation (Fig. 6) (Schier et al., 2020). These are the oldest confirmed negative Ce anomalies documented from unaltered drill core (Fig. 6), providing strong evidence for a primary oxygenic signal associated

with Mn deposition, and demonstrating that in the Transvaal Supergroup it appears that increasing Mn concentrations coincide with the onset and progression of the GOE.

The relative abundances of sedimentary Mn and Fe provide further information on depositional redox states and by extension the presence or absence of O_2 (Wang et al., 2022). For

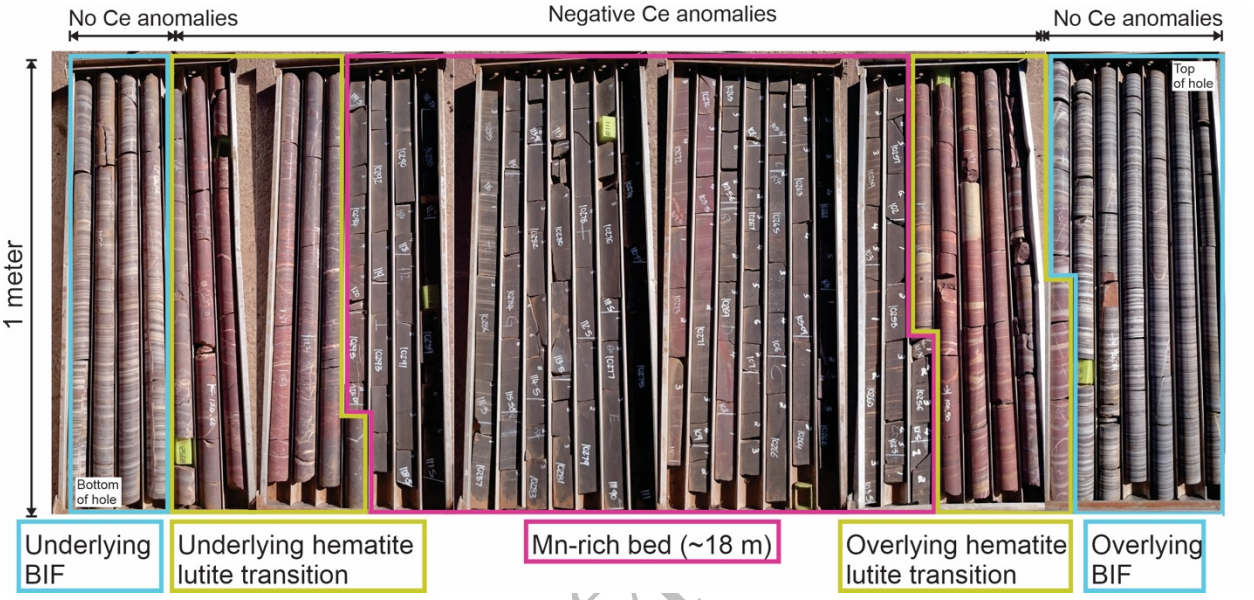

Figure 6. A combination of photographs of drill core intersecting the lower Hotazel Formation at Middelplaats Farm in the southern Kalahari Manganese Field, South Africa. Illustrated are the first (lowermost) banded iron formations to the left, the lower manganese bed in the middle, and the second banded iron formation to the right, along with the transitional hematite lutite beds below and above the lower manganese bed. Cerium anomalies, first reported by Schier et al. (2020), only occur in the hematite lutite and manganese beds.

instance, low Fe/Mn ratios in 2.95 Ga BIF from the Sinqeni Formation indicate enrichment of Mn relative to Fe and coincide with depleted Mo isotopes that require the adsorption of light Mo onto Mn oxides (Planavsky et al., 2014). This relationship would indicate that the contemporaneous seawater was at least mildly oxygenated, with limited free Fe(II). Other lines of independent evidence support this conclusion. For example, in the Sinqeni Formation, the interval with the highest Mn enrichment is also characterized by the lightest Fe isotope values (Planavsky et al.,

2014; Albut et al., 2019; Heard et al., 2021). Similarly, Wang et al. (2022) documented substantial shifts in the $\delta^{56}Fe$ values and Mn/Fe ratios of ~2.5–2.4 Ga iron formations in both western Australia and South Africa, which likely reflect changing marine redox conditions across large portions of the continental margins. Specifically, as $\delta^{56}Fe$ values in these iron formations become more negative towards ~2.4 Ga, Mn/Fe ratios become higher, and a negative correlation between Mn/Fe ratios and $\delta^{56}Fe$ values is observed for all iron formation samples across this interval (Wang et al., 2022). This is the product of gradually increasing seawater O_2 levels, where light Fe isotope values develop when the oxidation of Fe at the chemocline is not quantitative (e.g., Rouxel et al., 2005; Busigny et al., 2014; Hiebert et al., 2018). This possibility would suggest that Mn oxide deposition was most intense once water column Fe oxidation removed most Fe(II), allowing Mn oxide export to underlying sediments without extensive reduction by Fe(II).

As mentioned, there are a number of Phanerozoic Mn ore deposits that may contradict a purely oxidative control on the deposition of Mn deposits through time, at least from a first-order perspective, although the oceans may have remained anoxic at depth until well into the Paleozoic (Dahl et al., 2010; Lu et al., 2018; Sperling et al., 2015; Stolper and Keller, 2018). For instance, the Late Devonian Xialei Mn deposit in the Yougiang basin, South China block, is lower Famennian in age (~372 -358.9 Ma) (Yan et al., 2020). Manganese (II) carbonates and silicates in the Xialei Mn deposit petrographically pre-date the formation of pyrite, a result of Mn(IV) being a higher energy yielding a terminal electron acceptor compared to sulfate, and were likely deposited as Mn(IV)-oxides before undergoing diagenesis and subsequent hydrothermal alteration (Yan et al., 2020). This process is effectively analogous to that proposed for the Mn shuttle in the Archean to Paleoproterozoic coinciding with BIFs deposition where oxidized Mn(IV) deposited to the sediment undergo reduction during early diagenesis. Importantly, the Mn enrichments are

coupled to Mn(IV) oxide deposition. This episode of Mn oxide deposition may have been promoted by the establishment of anoxic conditions during the Fammennian (Late Devonian), allowing a build-up of appreciable dissolved Mn(II), similar to the Archean oceans prior to the GOE. This may also be interpreted as reflecting the oxygenation of the prior anoxic Paleozoic ocean and the ultimate establishment of well-oxygenated oceans (Dahl et al., 2010; Lu et al., 2018; Sperling et al., 2015; Stolper and Keller, 2018). Similarly, residual Mn(III)-bearing oxides and mixed valence Mn-silicates have been documented in both the Xialei Mn deposit and Permian Zunyi Mn deposit in South China, suggestive of primary Mn(IV) oxide reduction (Yan et al., 2022). Finally, recent parallels between petrographic microstructures observed in the Carboniferous Kalaatehe Formation and experimental incubations where Mn(IV) oxide reduction promotes Mn(II)-carbonate formation have also been documented, providing further support for the role of DMR in the formation of these massive ore deposits (Huang et al., 2022).

Two settings that may support the development of Mn deposits that warrant further consideration are O_2 minimum zones and euxinic settings (Maynard, 2010). Both of these environments may lead to the development of sedimentary Mn deposits, and both are intrinsically linked to primary production in the biosphere. Oxygen-minimum zones and euxinia develop on continental shelves and in restricted basins, respectively, due to high levels of primary productivity and flux of organic carbon to the seafloor. Here, we focus on the Carboniferous Zhaosu and Malkansu Mn deposits in China, as they offer interesting analogues to the Mn enrichments associated with O_2 minimum zones and euxinia, respectively (Dong et al., 2022, 2023). Both deposits are dominated by Mn(II)-carbonate minerals and multiple independent lines of evidence (e.g., Ce anomalies, C and Mo isotopes) indicate that the Mn(II)-carbonate ores were formed during diagenesis via the coupled oxidation of organic matter and reduction of Mn(IV)-oxides

764 deposited from an oxygenated water column. Specifically, the Malkansu Mn ore beds are hosted
765 within laminated, organic-rich mudstones (i.e., black shales) reflective of a relatively deep-water
766 depositional environment. Further, Fe speciation, coupled with a high abundance of small
767 framboidal pyrites (mean diameter ~5 μm), indicates that these black shales were deposited in
768 euxinic (H_2S-bearing) bottom waters. Combined, the Mn-ore intervals document the sharp
769 oxygenation of euxinic bottom waters, a process that might be induced by the periodic incursions
770 of oxic seawater associated with eustatic sea level rises (Dong et al., 2023). By contrast, the Zhaosu
771 Mn carbonate deposit occurs within a marine transgressive siliciclastic-carbonate succession.
772 Given the associated limestones with strongly negative Ce anomalies, an oxic-suboxic stratified
773 water column (most likely an O_2 minimum zone) might have characterized the Zhaosu basin during
774 Mn deposition (Dong et al., 2022). In both scenarios, Mn mineralization is driven by the presence
775 of an anoxic (or euxinic) water body underlying shallower oxic waters. While O_2 may not have
776 been the primary driver of Mn mineralization in these systems, the biosphere and O_2 certainly
777 played a role in generating the hydrographic conditions necessary for the development of these
778 sedimentary Mn deposits.

779 In Fayetteville Green Lake, New York (Herndon et al., 2018), and Brownie Lake,
780 Minnesota (Wittkop et al., 2020), primary Mn(II)-rich carbonates have been reported to form in
781 reducing waters below a chemocline. In both cases, Mn was associated with a carbonate sediment
782 phase, while Fe was more typically associated with sulfides. Additionally, in the Otter Lake,
783 Michigan, Mn enrichments in carbonates have also been documented (Wittkop et al., 2014).
784 However, these are present dominantly as manganoan siderites, which may point to previously
785 ferruginous conditions within the Otter Lake (Swanner et al., 2020). Consistent with these
786 observations, recent work has argued that Mn enrichments in the Griquatown and Kuruman iron

formations are the result of calcite precipitation and subsequent diagenetic replacement by ankerite and siderite (Siahi et al., 2020). Note that Carboniferous Mn-carbonate ores in the Longtou Deposit, China, preserved as rhodochrosite, manganoan calcite, and braunite laminae, have similarly been suggested to form via direct Mn-carbonate precipitation, driven by the influx of Mn-rich water masses, which led to the supersaturation and precipitation of Mn carbonates (F. Chen et al., 2022). The precipitation of the Longtou Mn-carbonate ores is in part attributed to the onset of anoxia driven by the upwelling of a hydrothermal water mass. This model for the Longtou Deposit is supported by seawater-like $\delta^{13}C$ values in the carbonates that suggest a primary formation pathway rather than DMR. These recent studies demonstrate the potential for formation of Mn carbonates within the water column and may have significant implications for Archean to Paleoproterozoic Mn deposits (Tsikos et al., 2022). In several cases, however, including Fayetteville Green Lake and Brownie Lake, the precipitation of Mn carbonate depends on a strong redoxcline being present and the decoupling of Fe and Mn by sulfur. This promotes the generation of high Mn/Fe ratios within the water column. In Brownie Lake, for instance, this is achieved through a combination of sulfur cycling and iron oxidation by either photoferrotrophs or microaerophilic iron-oxidizing bacteria and results in Mn(II) concentrations in excess of 100 μM (Wittkop et al., 2020). This observation may indicate that to some degree, oxidizing conditions or at least biological Fe oxidation are necessary for generating the conditions required for the precipitation of primary Mn carbonates. Whether or not these various models for primary Mn carbonates can be applied across the Archean to Paleoproterozoic record remains an avenue for future work. In any event, each of these scenarios points to some combination of O_2, biology, and hydrographic processes generating the conditions necessary for the formation of appreciable Mn enrichments.

5. Archean oxygenation and the GOE: Genomic, geochemical, and Mn oxide evidence

While the presence of Mn oxides, or their diagenetic derivatives, has often been used as evidence of oxygenation of at least portions of the environment in the Archean, reconstructing the protracted history of oxygenation (Fig. 4) is challenging. This is compounded by imprecise and often divergent molecular clock estimates for the rise of oxygenic photosynthesis in bacteria and either trace or cryptic geochemical signals. Divergent estimates for the rise of oxygenic photosynthetic lineages span a range of over a billion years (Fig. 4B), with estimates of 2.6–2.5 Ga based on the divergence between the Oxyphotobacteria and its sister lineage Melainabacteria (Shih et al., 2016) and ~2.3 Ga based on the divergence of stem cyanobacteria molecular clocks constrained by horizontal gene transfer (Magnabosco et al., 2018). Recent work, however, pushes the emergence of oxygenic photosynthesis back even further to the early Archean, perhaps >3.5 Ga, based on molecular clock estimates for the emergence of photosystem II, which is necessary to split water in photosynthetic pathways (Cardona et al., 2018). More recently, improved models imply the emergence of cyanobacteria in the early Archean with oxygenic photosynthesis arising in the Mesoarchean, hundreds of millions of years before the GOE (Fournier et al., 2021). The origin of oxygenic photosynthesis broadly corresponded with the emergence of stem group lineages of cyanobacteria and was followed by an interval of diversification that is the time equivalent to the GOE. Similarly, a recent phylogenomic study on oxygen-producing and -utilizing enzymes suggests a rapid proliferation of these enzymes around 3.1 Ga (Jabłońska and Tawfik, 2021). Taken together, and in light of the most recent analyses, molecular biological evidence points to photosynthetic oxygen production well before the GOE, thus supporting models for Archean

832 sedimentary Mn seafloor delivery and even enrichment based on the export of Mn oxides from at
833 least mildly oxygenated, relatively shallow-water columns.

834 There has also been a focus on using a diverse suite of geochemical tracers to reconstruct
835 Earth's oxygenation history (Fig. 4A) (see Catling and Zahnle (2020) and Lyons et al., (2021,
836 2014) for reviews). A more recent effort to reconstruct the history of Earth's oxygenation (Fig.
837 4A) has utilized machine learning approaches to estimating O_2 levels based on mafic igneous
838 geochemistry data, producing a remarkably similar history to that based on traditional sedimentary
839 proxies (G. Chen et al., 2022). Studies that have used sedimentary proxies have identified possible
840 indications of O_2 within the water column and atmosphere from as early as 3.8 to 3.7 Ga based on
841 positive chromium isotope ratios ($\delta^{53}Cr$) and elevated U/Th ratios in BIF samples from the Isua
842 Greenstone Belt (Frei et al., 2016). Positive $\delta^{53}Cr$ signals have also been observed in
843 contemporaneous 3.0 Ga paleosols and BIFs, which similarly imply free O_2 in Earth's surface
844 environments in the Mesoarchean (Crowe et al., 2013). However, the 3.0 Ga $\delta^{53}Cr$ compositions
845 in BIFs have recently been challenged, with indications that recent oxidative weathering of outcrop
846 rocks may have contributed to the positive $\delta^{53}Cr$ compositions in BIFs (Albut et al., 2018; Heard
847 et al., 2021). Critically, the large-scale generation of positively fractionated $\delta^{53}Cr$ likely requires
848 the presence of Mn oxides in continental weathering environments, as originally thought (Frei et
849 al., 2009) or may be generated during the rapid oxidation of Mn(II) and Cr(III) within the water
850 column (Miletto et al., 2021). In a similar fashion, Ce anomalies from outcrop samples of iron
851 formation of the 3.22 Ga Moodies Formation have recently been shown to reflect REE mobility
852 during more recent weathering (Bonnand et al., 2020), highlighting the potential dangers of later
853 overprints. Additional evidence for Archean O_2 comes from oxidative uranium cycling (Satkoski
854 et al., 2015) based on U-Th-Pb analyses of the 3.2 Ga Manzimnyama BIF, Fig Tree Group, South

855 Africa; putative cyanobacterial mats identified in the 3.22 Moodies Group, South Africa (Homann,
856 2019; Homann et al., 2018, 2015); elevated Mn/Fe ratios and a significant negative correlations
857 between Mn/Fe ratios and δ^{56}Fe values are observed in the ~3.22 Ga Moodies BIF and other BIFs
858 and exhalites (Hiebert et al., 2018; Wang et al., 2022) and Mn/Fe ratios and δ^{98}Mo in the ~2.95
859 Ga Sinqeni BIF (Planavsky et al., 2014) in South Africa; coupled S and Fe isotope values in pyrites
860 from shallow-water stromatolitic dolostones of the 3.0 Ga Nsuze Group in South Africa
861 (Eickmann et al., 2018); and the possibility that nitrate was available as an oxidant for organic
862 carbon remineralization in the ~2.9 Ga Nconga Formation in southern Africa (Smith et al., 2017).
863 A recent, detailed study of the Ijzermijn Iron Formation Bed part of the ~2.95 Ga Sinqeni
864 Formation (Smith and Beukes, 2023) provides further evidence for environmental oxidation
865 consistent with previous work on Mo isotopes on this formation (Albut et al., 2019; Planavsky et
866 al., 2014). Geochemical differences between localities along the paleo-shoreline and those more
867 distal are documented, with proximal settings being characterized by features such as C isotope
868 depletion in carbonates and higher MnO abundances (Smith and Beukes, 2023). These spatial
869 relations indicate that there was Mn(II) oxidation by O_2 and deposition of Mn oxides in proximal
870 settings, followed by subsequent diagenesis; for this to occur, Fe(II) had to have been removed by
871 oxidation in more distal settings (Smith and Beukes, 2023).

872 Given the above discussion of Mn oxides in the rock record and this brief history of Earth's
873 oxygenation, we can now attempt to answer the question: *Does the history of Mn oxides support*
874 *the protracted oxidation of Earth's surface environments in the build-up to the GOE?* An inverse
875 correlation between Mn oxides and molybdenum isotopes (δ^{98}Mo) is generated through the
876 negative fractionation of Mo during adsorption to Mn oxides, such that negative δ^{98}Mo values are
877 observed in samples of iron formations with the lowest Fe/Mn ratios. This relationship has been

observed in the 2.95 Ga Sinqeni Formation, suggesting that Mn oxide export and sedimentation delivered fractionated Mo to the sediments at the time of deposition (Planavsky et al., 2014). Despite studies such as these, however, the early history of oxygenation on Earth remains the focus of continued work. One challenging aspect is that many iron formations lack sedimentary structures, implying that deposition occurred below the wave base (e.g., Beukes and Gutzmer, 2008; Smith et al., 2013). This observation places deposition below ~100-150 m, and to some degree disconnects their deposition from the shallow oxidizing water expected at this point in Earth's history. Yet, Mn enrichments in the iron formations of the Witwatersrand Supergroup (Smith et al., 2013), the Sinqeni Formation (Albut et al., 2019; Planavsky et al., 2014; Ossa Ossa et al., 2019), and the Koegas and Hotazel formations (Wang et al., 2022) would require a substantial flux of Mn at depths below 150 m, given the lack of sedimentary structures, and by extension at least low levels of O_2 in the water column. Given the necessity for shallow waters with ambient O_2 in preserving sedimentary Mn oxide enrichments and the rise of Mn deposits preserved in the lead-up to the GOE, it is reasonable to conclude that large sedimentary Mn enrichments are linked, at least indirectly, to the presence of O_2 in the environment.

6. Conclusions

While Mn enrichments in ancient sedimentary successions are traditionally thought to reflect Earth's surface oxygenation, new observations suggest other possibilities. The potential for microbial anaerobic Mn oxidation in extant organisms and the demonstration of UV photooxidation insinuate that O_2-independent modes of Mn enrichment may have the potential to explain sedimentary Mn enrichments prior to the onset of oxygenic photosynthesis. However, although support for such pathways in laboratory settings is growing, combined consideration of

the well-known environmental geochemistry of Mn and ancient depositional conditions strongly implies that such anoxic pathways had little potential to drive large-scale Mn oxide deposition in the Archean. For example, anaerobic microbial oxidation has only been achieved in a sulphidic medium (Daye et al., 2019). That sulphide should result in appreciable iron? sulphide formation and deposition. However, such occurrences are not, for example, observed in the Witswatersrand-Mozaan succession (Smith et al., 2023) and Pongola Supergroup (Smith and Beukes, 2023; Smith et al., 2023). The same deficiencies apply to the Hotazel Formation, which contains little to no sulphide minerals. Moreover, these anaerobic pathways would be unable to account for the associated geochemical proxy records, including trace element and isotopic signals (e.g., Cr, Mo) that support environmental oxygenation in pre-GOE successions. Similarly, abiotic nucleation of Mn carbonates is challenging to reconcile with existing interpretations of depleted C isotope data that point toward dissimilatory reduction of Mn oxides. Moreover, abiotic oxidation of Mn(II) through photooxidation driven by UV light is unlikely in Archean marine settings. The low likelihood of photooxidation is suggested by the expected lack of rhodochrosite in the Archean surface ocean, the locus of photooxidation, and because seawater salinities are likely to limit the effectiveness of this pathway, as has been demonstrated previously for Fe. Given these considerations, it is likely that anoxic pathways were only minor contributors to the development of appreciable Mn enrichments.

Overall, the presence of Mn enrichments, along with other geochemical proxies for oxidizing conditions such as heavy Cr or light Mo isotopic compositions or enriched RSE abundances in shales, likely reflect oxygenated water columns. Importantly, regardless of the specific mechanism of oxidation, water column O_2 is almost certainly necessary to support Mn oxide transport to the seafloor. In keeping with this view, the close association between increasing

environmental oxidation in the Paleoproterozoic and Mn enrichment in sediments of the Transvaal Supergroup, notably the Hotazel Formation, suggests a causal relationship. Indeed, based on geochemical considerations, such as the ability of Fe(II) to reduce Mn(IV) oxides in the water column, it becomes apparent that preservation of large Mn enrichments almost certainly requires some degree of environmental oxygenation. Overall, this suggests that the presence of sedimentary Mn enrichments prior to the GOE requires bottom water O_2 or a redoxcline that sits near the seawater-sediment interface and would allow the export of Mn oxides. Such a model is consistent with the enrichment of Mn in Phanerozoic systems, which require oxygenated waters overlying either euxinic basins or O_2 minimum zones.

Based on the available data, we conclude that presence of Mn oxides before the rise of atmospheric O_2 and as early as 3.0 Ga is a direct result of the emergence of oxygenic photosynthesis and the onset of oxidative cycling of elements. Such a conclusion is entirely in line with recent molecular clocks that predict oxygenic photosynthesis by the Mesoarchean. Therefore, we contend that in combination with other geochemical proxies, the record of Mn enrichments in the Archean to Paleoproterozoic strongly reflects the incipient oxygenation of Earth's surface environments.

Acknowledgments

The authors thank Dillan Fitton for supplying the petrographic plate of the Hotazel Formation. The authors are grateful to Andrey Bekker and an anonymous reviewer for insightful comments that greatly improved the manuscript, and to Tim Kusky for editorial handling. LJR gratefully acknowledges support from the Natural Science and Engineering Research Council of Canada (NSERC) Discovery Grant program (RGPIN-2021-0523). BAB gratefully acknowledges the

947 support of an NSERC CGSD. CLP gratefully acknowledges the Royal Society Wolfson Research
948 Merit Award (WRM/FT/170005). WCL gratefully acknowledges support from from the National
949 Natural Science Foundation of China (grant 42150104) and Youth Innovation Promotion
950 Association, Chinese Academy of Sciences. Funding was provided by the NASA Interdisciplinary
951 Consortia for Astrobiology Research (ICAR program; TWL, NJP, and CTR).

952

953 **Author contributions**

954 LJR and MF conceived the study. All authors contributed to the discussion of ideas and writing
955 the manuscript.

956

957 **Competing Interests**

958 The authors declare no competing interests.

959

960 **References**

961
962

963 Albut, G., Babechuk, M.G., Kleinhanns, I.C., Benger, M., Beukes, N.J., Steinhilber, B., Smith,
964 A.J.B., Kruger, S.J., Schoenberg, R., 2018. Modern rather than Mesoarchaean oxidative
965 weathering responsible for the heavy stable Cr isotopic signatures of the 2.95 Ga old Ijzermijn
966 iron formation (South Africa). Geochim Cosmochim Ac 228, 157 189.
967 https://doi.org/10.1016/j.gca.2018.02.034

968 Albut, G., Kamber, B.S., Brüske, A., Beukes, N.J., Smith, A.J.B., Schoenberg, R., 2019. Modern
969 weathering in outcrop samples versus ancient paleoredox information in drill core samples
970 from a Mesoarchaean marine oxygen oasis in Pongola Supergroup, South Africa. Geochim
971 Cosmochim Ac 265, 330–353. https://doi.org/10.1016/j.gca.2019.09.001

972 Alcott, L.J., Mills, B.J.W., Poulton, S.W., 2019. Stepwise Earth oxygenation is an inherent
973 property of global biogeochemical cycling. Sci New York N Y 366, eaax6459.
974 https://doi.org/10.1126/science.aax6459

975 Anbar, A.D., Duan, Y., Lyons, T.W., Arnold, G.L., Kendall, B., Creaser, R.A., Kaufman, A.J.,
976 Gordon, G.W., Scott, C., Garvin, J., Buick, R., 2007. A Whiff of Oxygen Before the Great
977 Oxidation Event? Science 317, 1903–1906. https://doi.org/10.1126/science.1140325

978 Anbar, A.D., Holland, H.D., 1992. The photochemistry of manganese and the origin of banded
979 iron formations. Geochim Cosmochim Ac 56, 2595–2603. https://doi.org/10.1016/0016-
980 7037(92)90346-k

981 Bau, M., Alexander, B.W., 2006. Preservation of primary REE patterns without Ce anomaly
982 during dolomitization of Mid-Paleoproterozoic limestone and the potential re-establishment
983 of marine anoxia immediately after the" Great Oxidation Event". South African Journal of
984 Geology 109, 81 86.

985 Bau, M., Romer, R.L., Lüders, V., Beukes, N.J., 1999. Pb, O, C isotopes in silicified Mooidraai
986 dolomite (Transvaal Supergroup, South Africa): implications for the composition of
987 Paleoproterozoic seawater and “dating” the increase of oxygen in the Precambrian
988 atmosphere. Earth and Planetary Science Letters 174, 43–57.

989 Bekker, A., Karhu, J.A., Eriksson, K.A., Kaufman, A.J., 2003. Chemostratigraphy of
990 Paleoproterozoic carbonate successions of the Wyoming Craton: tectonic forcing of
991 biogeochemical change? Precambrian Res 120, 279–325. https://doi.org/10.1016/s0301-
992 9268(02)00164-x

993 Bekker, A., Krapež, B., Karhu, J.A., 2020. Correlation of the stratigraphic cover of the Pilbara
994 and Kaapvaal cratons recording the lead up to Paleoproterozoic Icehouse and the GOE. Earth-
995 sci Rev 211, 103389. https://doi.org/10.1016/j.earscirev.2020.103389

996 Bekker, A., Krapež, B., Karhu, J.A., Chamberlain, K., 2021. Reply to comment on “Bekker, A.,
997 Krapež, B., Karhu, J.A., 2020. Correlation of the stratigraphic cover of the Pilbara and
998 Kaapvaal cratons recording the lead up to Paleoproterozoic Icehouse and the GOE. Earth-
999 Science Reviews, 211, 103,389” by Pascal Philippot, Bryan A. Killingsworth, Jean-Louis
1000 Paquette, Svetlana Tessalina, Pierre Cartigny, Stefan V. Lalonde, Christophe Thomazo,
1001 Janaina N. Ávila, Vincent Busigny. Earth-sci Rev 218, 103607.
1002 https://doi.org/10.1016/j.earscirev.2021.103607

1003 Bekker, A., Planavsky, N.J., Krapez, B., Rasmussen, B., Hofmann, A., Slack, J.F., Rouxel, O.J.,
1004 Konhauser, K.O., 2014. Iron Formations: Their Origins and Implications for Ancient
1005 Seawater Chemistry, in: Treatise on Geochemistry. Elsevier, p. 561 628.
1006 https://doi.org/10.1016/b978-0-08-095975-7.00719-1

1007 Beukes, N., 1984. Sedimentology of the Kuruman and Griquatown iron-formations, Transvaal
1008 supergroup, Griqualand West, South Africa. Precambrian Res 24, 47 84.
1009 https://doi.org/10.1016/0301-9268(84)90069-x

1010 Beukes, N., Klein, C., Kaufman, A., Hayes, J., 1990. Carbonate petrography, kerogen
1011 distribution, and carbon and oxygen isotope variations in an Early Proterozoic transition from

limestone to iron-formation deposition, Transvaal Supergroup, South Africa. Econ Geol 85, 663 690. https://doi.org/10.2113/gsecongeo.85.4.663

Beukes, N.J., Gutzmer, J., 2008. Origin and paleoenvironmental significance of major iron formations at the Archean-Paleoproterozoic boundary. Society of Economic Geologists Reviews 15, 5 47.

Beukes, N.J., Swindell, E.P.W., Wabo, H., 2016. Manganese Deposits of Africa. Episodes 39, 285–317. https://doi.org/10.18814/epiiugs/2016/v39i2/95779

Boden, J.S., Konhauser, K.O., Robbins, L.J., Sánchez-Baracaldo, P., 2021. Timing the evolution of antioxidant enzymes in cyanobacteria. Nat Commun 12, 4742. https://doi.org/10.1038/s41467-021-24396-y

Boggs, S., 1995. Principles of Sedimentology and Stratigraphy. Prentice-Hall, New Jersey.

Bonnand, P., Lalonde, S.V., Boyet, M., Heubeck, C., Homann, M., Nonnotte, P., Foster, I., Konhauser, K.O., Köhler, I., 2020. Post-depositional REE mobility in a Paleoarchean banded iron formation revealed by La-Ce geochronology: A cautionary tale for signals of ancient oxygenation. Earth Planet Sc Lett 547, 116452. https://doi.org/10.1016/j.epsl.2020.116452

Boudreau, B.P., Mucci, A., Sundby, B., Luther, G.W., Silverberg, N., 1998. Comparative diagenesis at three sites on the Canadian continental margin. J Mar Res 56, 1259–1284. https://doi.org/10.1357/002224098765093634

Burdige, D.J., 1993. The biogeochemistry of manganese and iron reduction in marine sediments. Earth-sci Rev 35, 249–284. https://doi.org/10.1016/0012-8252(93)90040-e

Busigny, V., Lebeau, O., Ader, M., Krapež, B., Bekker, A., 2013. Nitrogen cycle in the Late Archean ferruginous ocean. Chem Geol 362, 115–130. https://doi.org/10.1016/j.chemgeo.2013.06.023

Busigny, V., Planavsky, N.J., Jezequel, D., Crowe, S.A., Louvat, P., Moureau, J., Viollier, E., Lyons, T.W., 2014. Iron isotopes in an Archean ocean analogue. Geochim Cosmochim Ac 133, 443 462. https://doi.org/10.1016/j.gca.2014.03.004

Cairns-Smith, A., 1978. Precambrian solution photochemistry, inverse segregation, and banded iron formations. Nature 276, 807 808.

Canfield, D., 1998. A new model for Proterozoic ocean chemistry. Nature 396, 450 453.

Cardona, T., Sánchez-Baracaldo, P., Rutherford, A.W., Larkum, A.W., 2018. Early Archean origin of Photosystem II. Geobiology 17, 21. https://doi.org/10.1111/gbi.12322

Catling, D.C., Zahnle, K.J., 2020. The Archean atmosphere. Sci Adv 6, eaax1420. https://doi.org/10.1126/sciadv.aax1420

Chaput, D.L., Fowler, A.J., Seo, O., Duhn, K., Hansel, C.M., Santelli, C.M., 2019. Mn oxide formation by phototrophs: Spatial and temporal patterns, with evidence of an enzymatic superoxide-mediated pathway. Sci Rep-uk 9, 18244. https://doi.org/10.1038/s41598-019-54403-8

Chen, F., Pufahl, P.K., Wang, Q., Matheson, E.J., Shabaga, B.M., Zhang, Q., Zeng, Y., Le, X., Ruan, D., Zhao, Y., 2022. A New Model for the Genesis of Carboniferous Mn Ores, Longtou Deposit, South China Block. Econ Geol 117, 107–125. https://doi.org/10.5382/econgeo.4855

Chen, G., Cheng, Q., Lyons, T.W., Shen, J., Agterberg, F., Huang, N., Zhao, M., 2022. Reconstructing Earth's atmospheric oxygenation history using machine learning. Nat Commun 13, 5862. https://doi.org/10.1038/s41467-022-33388-5

Chernev, P., Fischer, S., Hoffmann, J., Oliver, N., Assunção, R., Yu, B., Burnap, R.L., Zaharieva, I., Nürnberg, D.J., Haumann, M., Dau, H., 2020. Light-driven formation of manganese oxide by today's photosystem II supports evolutionarily ancient manganese-oxidizing photosynthesis. Nat Commun 11, 6110. https://doi.org/10.1038/s41467-020-19852-0

Cornell, D.H., Schütte, S.S., Eglington, B.L., 1996. The Ongeluk basaltic andesite formation in Griqualand West, South Africa: submarine alteration in a 2222 Ma proterozoic sea. Precambrian Res 79, 101–123. https://doi.org/10.1016/0301-9268(95)00090-9

Crowe, S.A., Canfield, D.E., Mucci, A., Sundby, B., Maranger, R., 2012. Anammox, denitrification and fixed-nitrogen removal in sediments from the Lower St. Lawrence Estuary. Biogeosciences 9, 4309–4321. https://doi.org/10.5194/bg-9-4309-2012

Crowe, S.A., Døssing, L.N., Beukes, N.J., Bau, M., Kruger, S.J., Frei, R., Canfield, D.E., 2013. Atmospheric oxygenation three billion years ago. Nature 501, 535 538. https://doi.org/10.1038/nature12426

Crowe, S.A., Jones, C., Katsev, S., Magen, C., O'Neill, A.H., Sturm, A., Canfield, D.E., Haffner, G.D., Mucci, A., Sundby, B., Fowle, D.A., 2008. Photoferrotrophs thrive in an Archean Ocean analogue. Proc National Acad Sci 105, 15938 15943. https://doi.org/10.1073/pnas.0805313105

Crowe, S.A., Paris, G., Katsev, S., Jones, C., Kim, S.-T., Zerkle, A.L., Nomosatryo, S., Fowle, D.A., Adkins, J.F., Sessions, A.L., Farquhar, J., Canfield, D.E., 2014. Sulfate was a trace constituent of Archean seawater. Science 346, 735 739. https://doi.org/10.1126/science.1258966

Dahl, T.W., Hammarlund, E.U., Anbar, A.D., Bond, D.P.G., Gill, B.C., Gordon, G.W., Knoll, A.H., Nielsen, A.T., Schovsbo, N.H., Canfield, D.E., 2010. Devonian rise in atmospheric oxygen correlated to the radiations of terrestrial plants and large predatory fish. Proc National Acad Sci 107, 17911 17915. https://doi.org/10.1073/pnas.1011287107

Davison, W., 1993. Iron and manganese in lakes. Earth-sci Rev 34, 119–163. https://doi.org/10.1016/0012-8252(93)90029-7

Daye, M., Klepac-Ceraj, V., Pajusalu, M., Rowland, S., Farrell-Sherman, A., Beukes, N., Tamura, N., Fournier, G., Bosak, T., 2019. Light-driven anaerobic microbial oxidation of manganese. Nature 576, 311–314. https://doi.org/10.1038/s41586-019-1804-0

Diaz, J.M., Hansel, C.M., Voelker, B.M., Mendes, C.M., Andeer, P.F., Zhang, T., 2013. Widespread Production of Extracellular Superoxide by Heterotrophic Bacteria. Science 340, 1223–1226. https://doi.org/10.1126/science.1237331

Diem, D., Stumm, W., 1984. Is dissolved Mn2+ being oxidized by O2 in absence of Mn-bacteria or surface catalysts? Geochim Cosmochim Ac 48, 1571–1573. https://doi.org/10.1016/0016-7037(84)90413-7

Dong, Z., Peng, Z., Wang, C., Zhang, B., Zhang, LianChang, Li, J., Zhang, X., Li, W., Zhang, Le, 2022. Insight into the genesis of the Zhaosu Carboniferous Mn carbonate deposit (NW China): constraints from petrography, geochemistry, and C–Mo isotopes. Mineral. Deposita 57, 1269–1289. https://doi.org/10.1007/s00126-022-01105-3

Dong, Z.-G., Peng, Z.-D., Robbins, L.J., Konhauser, K.O., Zhang, B.-L., Zhang, L.-C., Li, J., Li, W.-J., Zhang, L., Wang, C.-L., 2023. Episodic ventilation of euxinic bottom waters triggers the formation of black shale-hosted Mn carbonate deposits. Geochim Cosmochim Ac 341, 132–149. https://doi.org/10.1016/j.gca.2022.11.027

Duckworth, O.W., Sposito, G., 2005. Siderophore−Manganese(III) Interactions. I. Air-Oxidation of Manganese(II) Promoted by Desferrioxamine B. Environ Sci Technol 39, 6037–6044. https://doi.org/10.1021/es050275k

Ehrenreich, A., Widdel, F., 1994. Anaerobic oxidation of ferrous iron by purple bacteria, a new type of phototrophic metabolism. Applied and Environmental Microbiology 60, 4517 4526.

Ehrlich, H.L., 1987. Manganese oxide reduction as a form of anaerobic respiration. Geomicrobiol J 5, 423–431. https://doi.org/10.1080/01490458709385977

Eickmann, B., Hofmann, A., Wille, M., Bui, T.H., Wing, B.A., Schoenberg, R., 2018. Isotopic evidence for oxygenated Mesoarchaean shallow oceans. Nat Geosci 289, 765. https://doi.org/10.1038/s41561-017-0036-x

Elderfield, H., 1981. Metal-organic associations in interstitial waters of Narragansett Bay sediments. Am J Sci 281, 1184–1196. https://doi.org/10.2475/ajs.281.9.1184

Eriksson, P.G., Altermann, W., Hartzer, F.J., 2006. The Transvaal supergroup and its precursors, in: Johnson, M.R., Anhaeusser, C.R., Thomas, R.J. (Eds.), The Geology of South Africa. Geological Society of South Africa, Johannesburg, Council for Geoscience, Pretoria, pp. 237–260.

Fairey, B., Tsikos, H., Corfu, F., Polteau, S., 2013. U–Pb systematics in carbonates of the Postmasburg Group, Transvaal Supergroup, South Africa: Primary versus metasomatic controls. Precambrian Res 231, 194–205. https://doi.org/10.1016/j.precamres.2013.03.010

Farquhar, J., Bao, H., Thiemens, M., 2000. Atmospheric Influence of Earth's Earliest Sulfur Cycle. Science 289, 756–758. https://doi.org/10.1126/science.289.5480.756

Farquhar, J., Zerkle, A.L., Bekker, A., 2011. Geological constraints on the origin of oxygenic photosynthesis. Photosynth Res 107, 11 36. https://doi.org/10.1007/s11120-010-9594-0

Fischer, W., Schroeder, S., Lacassie, J., Beukes, N., Goldberg, T., Strauss, H., Horstmann, U., Schrag, D., Knoll, A.H., 2009. Isotopic constraints on the Late Archean carbon cycle from the Transvaal Supergroup along the western margin of the Kaapvaal Craton, South Africa. Precambrian Res 169, 15 27. https://doi.org/10.1016/j.precamres.2008.10.010

Fischer, W.W., Hemp, J., Johnson, J.E., 2015. Manganese and the Evolution of Photosynthesis. Origins Life Evol B 45, 351–357. https://doi.org/10.1007/s11084-015-9442-5

Fournier, G.P., Moore, K.R., Rangel, L.T., Payette, J.G., Momper, L., Bosak, T., 2021. The Archean origin of oxygenic photosynthesis and extant cyanobacterial lineages. Proc Royal Soc B 288, 20210675. https://doi.org/10.1098/rspb.2021.0675

Frei, R., Crowe, S.A., Bau, M., Polat, A., Fowle, D.A., 2016. Oxidative elemental cycling under the low O2 Eoarchean atmosphere. Sci Rep 6, 21058. https://doi.org/10.1038/srep21058

Frei, R., Gaucher, C., Poulton, S.W., Canfield, D.E., 2009. Fluctuations in Precambrian atmospheric oxygenation recorded by chromium isotopes. Nature 461, 250 253. https://doi.org/10.1038/nature08266

Froelich, P.N., Klinkhammer, G.P., Bender, M.L., Luedtke, N.A., Heath, G.R., Cullen, D., Dauphin, P., Hammond, D., Hartman, B., Maynard, V., 1979. Early oxidation of organic matter in pelagic sediments of the eastern equatorial Atlantic: suboxic diagenesis. Geochim Cosmochim Ac 43, 1075–1090. https://doi.org/10.1016/0016-7037(79)90095-4

Garvin, J., Buick, R., Anbar, A.D., Arnold, G.L., Kaufman, A.J., 2009. Isotopic Evidence for an Aerobic Nitrogen Cycle in the Latest Archean. Science 323, 1045 1048. https://doi.org/10.1126/science.1165675

Godfrey, L.V., Falkowski, P.G., 2009. The cycling and redox state of nitrogen in the Archaean ocean. Nat Geosci 2, 725–729. https://doi.org/10.1038/ngeo633

Godwin, C.M., Zehnpfennig, J.R., Learman, D.R., 2020. Biotic and Abiotic Mechanisms of Manganese (II) Oxidation in Lake Erie. Frontiers Environ Sci 8, 57. https://doi.org/10.3389/fenvs.2020.00057

1149 Gumsley, A.P., Chamberlain, K.R., Bleeker, W., Söderlund, U., Kock, M.O. de, Larsson, E.R.,
1150 Bekker, A., 2017. Timing and tempo of the Great Oxidation Event. Proc National Acad Sci
1151 114, 1811 1816. https://doi.org/10.1073/pnas.1608824114

1152 Gutzmer, J., Beukes, N.J., 1996. Mineral paragenesis of the Kalahari managanese field, South
1153 Africa. Ore Geol Rev 11, 405–428. https://doi.org/10.1016/s0169-1368(96)00011-x

1154 Gutzmer, J., Beukes, N.J., 1995. Fault-controlled metasomatic alteration of early Proterozoic
1155 sedimentary manganese ores in the Kalahari manganese field, South Africa. Econ Geol 90,
1156 823–844. https://doi.org/10.2113/gsecongeo.90.4.823

1157 Habicht, K.S., Gade, M., Thamdrup, B., Berg, P., Canfield, D.E., 2002. Calibration of Sulfate
1158 Levels in the Archean Ocean. Science 298, 2372–2374.
1159 https://doi.org/10.1126/science.1078265

1160 Halevy, I., 2013. Production, preservation, and biological processing of mass-independent sulfur
1161 isotope fractionation in the Archean surface environment. Proc National Acad Sci 110,
1162 17644–17649. https://doi.org/10.1073/pnas.1213148110

1163 Halevy, I., Bachan, A., 2017. The geologic history of seawater pH. Science 355, 1069 1071.
1164 https://doi.org/10.1126/science.aal4151

1165 Hansel, C.M., 2017. Chapter Two Manganese in Marine Microbiology. Adv Microb Physiol 70,
1166 37–83. https://doi.org/10.1016/bs.ampbs.2017.01.005

1167 Hansel, C.M., Zeiner, C.A., Santelli, C.M., Webb, S.M., 2012. Mn(II) oxidation by an
1168 ascomycete fungus is linked to superoxide production during asexual reproduction. Proc
1169 National Acad Sci 109, 12621–12625. https://doi.org/10.1073/pnas.1203885109

1170 Hayes, C.T., Anderson, R.F., Fleisher, M.Q., Vivancos, S.M., Lam, P.J., Ohnemus, D.C., Huang,
1171 K.-F., Robinson, L.F., Lu, Y., Cheng, H., Edwards, R.L., Moran, S.B., 2015. Intensity of Th
1172 and Pa scavenging partitioned by particle chemistry in the North Atlantic Ocean. Mar Chem
1173 170, 49–60. https://doi.org/10.1016/j.marchem.2015.01.006

1174 Heard, A.W., Aarons, S.M., Hofmann, A., He, X., Ireland, T., Bekker, A., Qin, L., Dauphas, N.,
1175 2021. Anoxic continental surface weathering recorded by the 2.95 Ga Denny Dalton Paleosol
1176 (Pongola Supergroup, South Africa). Geochim Cosmochim Ac 295, 1–23.
1177 https://doi.org/10.1016/j.gca.2020.12.005

1178 Henkel, J.V., Dellwig, O., Pollehne, F., Herlemann, D.P.R., Leipe, T., Schulz-Vogt, H.N., 2019.
1179 A bacterial isolate from the Black Sea oxidizes sulfide with manganese(IV) oxide. Proc
1180 National Acad Sci 116, 12153–12155. https://doi.org/10.1073/pnas.1906000116

1181 Herndon, E.M., Havig, J.R., Singer, D.M., McCormick, M.L., Kump, L.R., 2018. Manganese
1182 and iron geochemistry in sediments underlying the redox-stratified Fayetteville Green Lake.
1183 Geochim Cosmochim Ac 231, 50–63. https://doi.org/10.1016/j.gca.2018.04.013

1184 Holland, H.D., 1984. Oxygen in the Precambrian Atmosphere: Evidence from Marine
1185 Environments, in: The Chemical Evolution of the Atmosphere and Oceans. P. 337 440.

1186 Homann, M., 2019. Earliest life on earth: Evidence from the Barberton Greenstone Belt, South
1187 Africa. Earth-sci Rev 102888. https://doi.org/10.1016/j.earscirev.2019.102888

1188 Homann, M., Heubeck, C., Airo, A., Tice, M.M., 2015. Morphological adaptations of 3.22 Ga-
1189 old tufted microbial mats to Archean coastal habitats (Moodies Group, Barberton Greenstone
1190 Belt, South Africa). Precambrian Res 266, 47 64.
1191 https://doi.org/10.1016/j.precamres.2015.04.018

1192 Homann, M., Sansjofre, P., Zuilen, M.V., Heubeck, C., Gong, J., Killingsworth, B., Foster, I.S.,
1193 Airo, A., Kranendonk, M.J.V., Ader, M., Lalonde, S.V., 2018. Microbial life and
1194 biogeochemical cycling on land 3,220 million years ago. Nat Geosci 537, 1 8.
1195 https://doi.org/10.1038/s41561-018-0190-9

1196 Huang, Q., Pi, D.-H., Jiang, S.-Y., Liu, D., Yan, H., Mänd, K., Kirsimäe, K., Bishop, B.,
1197 Robbins, L.J., Yang, S.-S., 2022. The dual role of microbes in the formation of the Malkantu
1198 manganese carbonate deposit, NW China: Petrographic, geochemical, and experimental
1199 evidence. Chem Geol 606, 120992. https://doi.org/10.1016/j.chemgeo.2022.120992

1200 Hulth, S., Aller, R.C., Gilbert, F., 1999. Coupled anoxic nitrification/manganese reduction in
1201 marine sediments. Geochim Cosmochim Ac 63, 49–66. https://doi.org/10.1016/s0016-
1202 7037(98)00285-3

1203 Jabłońska, J., Tawfik, D.S., 2021. The evolution of oxygen-utilizing enzymes suggests early
1204 biosphere oxygenation. Nat Ecol Evol 1–7. https://doi.org/10.1038/s41559-020-01386-9

1205 Jeandel, C., Loeff, M.R. van der, Lam, P.J., Roy-Barman, M., Sherrell, R.M., Kretschmer, S.,
1206 German, C., Dehairs, F., 2015. What did we learn about ocean particle dynamics in the
1207 GEOSECS–JGOFS era? Prog Oceanogr 133, 6–16.
1208 https://doi.org/10.1016/j.pocean.2014.12.018

1209 Johnson, C.M., Beard, B.L., Klein, C., Beukes, N.J., Roden, E.E., 2008. Iron isotopes constrain
1210 biologic and abiologic processes in banded iron formation genesis. Geochim Cosmochim Ac
1211 72, 151 169. https://doi.org/10.1016/j.gca.2007.10.013

1212 Johnson, J.E., Webb, S.M., Thomas, K., Ono, S., Kirschvink, J.L., Fischer, W.W., 2013.
1213 Manganese-oxidizing photosynthesis before the rise of cyanobacteria, in: Proceedings of the
1214 National Academy of Sciences. Pp. 11238–11243. https://doi.org/10.1073/pnas.1305530110

1215 Jones, C., Crowe, S.A., Sturm, A., Leslie, K.L., MacLean, L.C.W., Katsev, S., Henny, C., Fowle,
1216 D.A., Canfield, D.E., 2011. Biogeochemistry of manganese in ferruginous Lake Matano,
1217 Indonesia. Biogeosciences 8, 2977–2991. https://doi.org/10.5194/bg-8-2977-2011

1218 Jones, M.R., Luther, G.W., Tebo, B.M., 2020. Distribution and concentration of soluble
1219 manganese(II), soluble reactive Mn(III)-L, and particulate MnO2 in the Northwest Atlantic
1220 Ocean. Mar Chem 226, 103858. https://doi.org/10.1016/j.marchem.2020.103858

1221 Jung, H., Chadha, T.S., Kim, D., Biswas, P., Jun, Y.-S., 2017. Photochemically assisted fast
1222 abiotic oxidation of manganese and formation of δ-MnO 2 nanosheets in nitrate solution.
1223 Chem Commun 53, 4445–4448. https://doi.org/10.1039/c7cc00754j

1224 Jung, H., Snyder, C., Xu, W., Wen, K., Zhu, M., Li, Y., Lu, A., Tang, Y., 2021a. Photocatalytic
1225 Oxidation of Dissolved Mn2+ by TiO2 and the Formation of Tunnel Structured Manganese
1226 Oxides. Acs Earth Space Chem 5, 2105–2114.
1227 https://doi.org/10.1021/acsearthspacechem.1c00154

1228 Jung, H., Xu, X., Wan, B., Wang, Q., Borkiewicz, O.J., Li, Y., Chen, H., Lu, A., Tang, Y.,
1229 2021b. Photocatalytic oxidation of dissolved Mn(II) on natural iron oxide minerals. Geochim
1230 Cosmochim Ac 312, 343–356. https://doi.org/10.1016/j.gca.2021.07.023

1231 Junta, J.L., Hochella, M.F., 1994. Manganese (II) oxidation at mineral surfaces: A microscopic
1232 and spectroscopic study. Geochim Cosmochim Ac 58, 4985–4999.
1233 https://doi.org/10.1016/0016-7037(94)90226-7

1234 Katsev, S., Rancourt, D.G., L'Heureux, I., 2004. dSED: a database tool for modeling sediment
1235 early diagenesis. Comput Geosci 30, 959–967. https://doi.org/10.1016/j.cageo.2004.06.005

1236 Kendall, B., Acken, D. van, Creaser, R.A., 2013. Depositional age of the early Paleoproterozoic
1237 Klipputs Member, Nelani Formation (Ghaap Group, Transvaal Supergroup, South Africa) and
1238 implications for low-level Re–Os geochronology and Paleoproterozoic global correlations.
1239 Precambrian Res 237, 1–12. https://doi.org/10.1016/j.precamres.2013.08.002

1240 Kendall, B., Creaser, R.A., Reinhard, C.T., Lyons, T.W., Anbar, A.D., 2015. Transient episodes
1241 of mild environmental oxygenation and oxidative continental weathering during the late
1242 Archean. Sci Adv 1, e1500777 e1500777. https://doi.org/10.1126/sciadv.1500777

1243 Kiratli, N., Ergin, M., 1996. Partitioning of heavy metals in surface Black Sea sediments. Appl
1244 Geochem 11, 775–788. https://doi.org/10.1016/s0883-2927(96)00037-6

1245 Konhauser, K.O., Amskold, L.A., Lalonde, S.V., Posth, N., Kappler, A., Anbar, A.D., 2007.
1246 Decoupling photochemical Fe (II) oxidation from shallow-water BIF deposition. Earth Planet
1247 Sc Lett 258, 87 100. https://doi.org/10.1016/j.epsl.2007.03.026

1248 Konhauser, K.O., Planavsky, N.J., Hardisty, D.S., Robbins, L.J., Warchola, T.J., Haugaard, R.,
1249 Lalonde, S.V., Partin, C.A., Oonk, P.B.H., Tsikos, H., Lyons, T.W., Bekker, A., Johnson,
1250 C.M., 2017. Iron formations: A global record of Neoarchaean to Palaeoproterozoic
1251 environmental history. Earth-sci Rev 172, 140 177.
1252 https://doi.org/10.1016/j.earscirev.2017.06.012

1253 Krauskopf, K.B., 1957. Separation of manganese from iron in sedimentary processes. Geochim
1254 Cosmochim Ac 12, 61–84. https://doi.org/10.1016/0016-7037(57)90018-2

1255 Kunzmann, M., Gutzmer, J., Beukes, N.J., Halverson, G.P., 2014. Depositional Environment and
1256 Lithostratigraphy of the Paleoproterozoic Mooidraai Formation, Kalahari Manganese Field,
1257 South Africa. S Afr J Geol 117, 173–192. https://doi.org/10.2113/gssajg.117.2.173

1258 Lalonde, K., Mucci, A., Ouellet, A., Gélinas, Y., 2012. Preservation of organic matter in
1259 sediments promoted by iron. Nature 483, 198–200. https://doi.org/10.1038/nature10855

1260 Lambrecht, N., Wittkop, C., Katsev, S., Fakhraee, M., Swanner, E.D., 2018. Geochemical
1261 Characterization of Two Ferruginous Meromictic Lakes in the Upper Midwest, USA. J
1262 Geophys Res Biogeosciences 123, 3403–3422. https://doi.org/10.1029/2018jg004587

1263 Lantink, M.L., Davies, J.H.F.L., Mason, P.R.D., Schaltegger, U., Hilgen, F.J., 2019. Climate
1264 control on banded iron formations linked to orbital eccentricity. Nat Geosci 12, 369–374.
1265 https://doi.org/10.1038/s41561-019-0332-8

1266 Learman, D.R., Voelker, B.M., Vazquez-Rodriguez, A.I., Hansel, C.M., 2011. Formation of
1267 manganese oxides by bacterially generated superoxide. Nat Geosci 4, 95–98.
1268 https://doi.org/10.1038/ngeo1055

1269 Lepland, A., Stevens, R.L., 1998. Manganese authigenesis in the Landsort Deep, Baltic Sea. Mar
1270 Geol 151, 1–25. https://doi.org/10.1016/s0025-3227(98)00046-2

1271 Lewis, B.L., Landing, W.M., 1991. The biogeochemistry of manganese and iron in the Black
1272 Sea. Deep Sea Res Part Oceanogr Res Pap 38, S773–S803. https://doi.org/10.1016/s0198-
1273 0149(10)80009-3

1274 Liu, W., Hao, J., Elzinga, E.J., Piotrowiak, P., Nanda, V., Yee, N., Falkowski, P.G., 2020.
1275 Anoxic photogeochemical oxidation of manganese carbonate yields manganese oxide. Proc
1276 National Acad Sci 117, 22698–22704. https://doi.org/10.1073/pnas.2002175117

1277 Lu, W., Ridgwell, A., Thomas, E., Hardisty, D.S., Luo, G., Algeo, T.J., Saltzman, M.R., Gill,
1278 B.C., Shen, Y., Ling, H.-F., Edwards, C.T., Whalen, M.T., Zhou, X., Gutchess, K.M., Jin, L.,
1279 Rickaby, R.E.M., Jenkyns, H.C., Lyons, T.W., Lenton, T.M., Kump, L.R., Lu, Z., 2018. Late
1280 inception of a resiliently oxygenated upper ocean. Science 5, eaar5372 177.
1281 https://doi.org/10.1126/science.aar5372

1282 Luff, R., Moll, A., 2004. Seasonal dynamics of the North Sea sediments using a three-
1283 dimensional coupled sediment–water model system. Cont Shelf Res 24, 1099–1127.
1284 https://doi.org/10.1016/j.csr.2004.03.010

1285 Lyons, T.W., Diamond, C.W., Konhauser, K.O., 2020. Shedding light on manganese cycling in
1286 the early oceans. Proc National Acad Sci 117, 25960–25962.
1287 https://doi.org/10.1073/pnas.2016447117

Lyons, T.W., Diamond, C.W., Planavsky, N.J., Reinhard, C.T., Li, C., 2021. Oxygenation, Life, and the Planetary System during Earth's Middle History: An Overview. Astrobiology 21, 906–923. https://doi.org/10.1089/ast.2020.2418

Lyons, T.W., Reinhard, C.T., Planavsky, N.J., 2014. The rise of oxygen in Earth's early ocean and atmosphere. Nature 506, 307 315. https://doi.org/10.1038/nature13068

Madison, A.S., Tebo, B.M., Mucci, A., Sundby, B., III, G.W.L., 2013. Abundant Porewater Mn(III) Is a Major Component of the Sedimentary Redox System. Science 341, 875–878. https://doi.org/10.1126/science.1241396

Magnabosco, C., Moore, K.R., Wolfe, J.M., Fournier, G.P., 2018. Dating phototrophic microbial lineages with reticulate gene histories. Geobiology 16, 179 189. https://doi.org/10.1111/gbi.12273

Mänd, K., Lalonde, S.V., Robbins, L.J., Thoby, M., Paiste, K., Kreitsmann, T., Paiste, P., Reinhard, C.T., Romashkin, A.E., Planavsky, N.J., Kirsimäe, K., Lepland, A., Konhauser, K.O., 2020. Palaeoproterozoic oxygenated oceans following the Lomagundi–Jatuli Event. Nat Geosci 13, 302–306. https://doi.org/10.1038/s41561-020-0558-5

Maynard, J.B., 2010. The Chemistry of Manganese Ores through Time: A Signal of Increasing Diversity of Earth-Surface Environments. Econ Geol 105, 535–552. https://doi.org/10.2113/gsecongeo.105.3.535

Means, J.L., Crerar, D.A., Borcsik, M.P., Duguid, J.O., 1978. Radionuclide adsorption by manganese oxides and implications for radioactive waste disposal. Nature 274, 44–47. https://doi.org/10.1038/274044a0

Mettam, C., Zerkle, A.L., Claire, M.W., Prave, A.R., Poulton, S.W., Junium, C.K., 2019. Anaerobic nitrogen cycling on a Neoarchaean ocean margin. Earth Planet Sc Lett 527, 115800. https://doi.org/10.1016/j.epsl.2019.115800

Miletto, M., Wang, X., Planavsky, N.J., Luther, G.W., Lyons, T.W., Tebo, B.M., 2021. Marine microbial Mn(II) oxidation mediates Cr(III) oxidation and isotope fractionation. Geochim Cosmochim Ac 297, 101–119. https://doi.org/10.1016/j.gca.2021.01.008

Murray, J.W., 1975. The interaction of metal ions at the manganese dioxide-solution interface. Geochim Cosmochim Ac 39, 505–519. https://doi.org/10.1016/0016-7037(75)90103-9

Nealson, K.H., 2006. The Prokaryotes, Volume 5: Proteobacteria: Alpha and Beta Subclasses 222–231. https://doi.org/10.1007/0-387-30745-1_11

Nico, P.S., Anastasio, C., Zasoski, R.J., 2002. Rapid photo-oxidation of Mn(II) mediated by humic substances. Geochim Cosmochim Ac 66, 4047–4056. https://doi.org/10.1016/s0016-7037(02)01001-3

Olson, J.M., 1970. The Evolution of Photosynthesis. Science 168, 438–446. https://doi.org/10.1126/science.168.3930.438

Olson, S.L., Kump, L.R., Kasting, J.F., 2013. Quantifying the areal extent and dissolved oxygen concentrations of Archean oxygen oases. Chem Geol 362, 35 43. https://doi.org/10.1016/j.chemgeo.2013.08.012

Ossa Ossa, F., Hofmann, A., Spangenberg, J.E., Poulton, S.W., Stüeken, E.E., Schoenberg, R., Eickmann, B., Wille, M., Butler, M., Bekker, A., 2019. Limited oxygen production in the Mesoarchean ocean. Proc National Acad Sci 116, 6647–6652. https://doi.org/10.1073/pnas.1818762116

Ossa Ossa, F., Spangenberg, J.E., Bekker, A., König, S., Stüeken, E.E., Hofmann, A., Poulton, S.W., Yierpan, A., Varas-Reus, M.I., Eickmann, B., Andersen, M.B., Schoenberg, R., 2022. Moderate levels of oxygenation during the late stage of Earth's Great Oxidation Event. Earth Planet Sc Lett 594, 117716. https://doi.org/10.1016/j.epsl.2022.117716

Ostrander, C.M., Nielsen, S.G., Owens, J.D., Kendall, B., Gordon, G.W., Romaniello, S.J., Anbar, A.D., 2019. Fully oxygenated water columns over continental shelves before the Great Oxidation Event. Nat Geosci 12, 186–191. https://doi.org/10.1038/s41561-019-0309-7

Philippot, P., Ávila, J.N., Killingsworth, B.A., Tessalina, S., Baton, F., Caquineau, T., Muller, É., Pecoits, E., Cartigny, P., Lalonde, S.V., Ireland, T.R., Thomazo, C., Kranendonk, M.J., Busigny, V., 2018. Globally asynchronous sulphur isotope signals require re-definition of the Great Oxidation Event. Nat Commun 9, 2245. https://doi.org/10.1038/s41467-018-04621-x

Philippot, P., Killingsworth, B.A., Paquette, J.-L., Tessalina, S., Cartigny, P., Lalonde, S.V., Thomazo, C., Ávila, J.N., Busigny, V., 2021. Comment on "Correlation of the stratigraphic cover of the Pilbara and Kaapvaal cratons recording the lead up to Paleoproterozoic Icehouse and the GOE" by Andrey Bekker, Bryan Krapež, and Juha A. Karhu, 2020, Earth Science Reviews, https://doi.org/10.1016/j.earscirev.2020.103389. Earth-sci Rev 218, 103594. https://doi.org/10.1016/j.earscirev.2021.103594

Pickard, A., 2003. SHRIMP U-Pb zircon ages for the Palaeoproterozoic Kuruman Iron Formation, Northern Cape Province, South Africa: evidence for simultaneous BIF deposition on Kaapvaal and Pilbara Cratons. Precambrian Res 125, 275 315. https://doi.org/10.1016/s0301-9268(03)00113-x

Planavsky, N.J., Asael, D., Hofmann, A., Reinhard, C.T., Lalonde, S.V., Knudsen, A., Wang, X., Ossa, F.O., Pecoits, E., Smith, A.J.B., Beukes, N.J., Bekker, A., Johnson, T.M., Konhauser, K.O., Lyons, T.W., Rouxel, O.J., 2014. Evidence for oxygenic photosynthesis half a billion years before the Great Oxidation Event. Nat Geosci 7, 283 286. https://doi.org/10.1038/ngeo2122

Planavsky, N.J., Cole, D.B., Isson, T.T., Reinhard, C.T., Crockford, P.W., Sheldon, N.D., Lyons, T.W., 2018. A case for low atmospheric oxygen levels during Earth's middle history. Emerg Top Life Sci 256, ETLS20170161 11. https://doi.org/10.1042/etls20170161

Poulton, S.W., Bekker, A., Cumming, V.M., Zerkle, A.L., Canfield, D.E., Johnston, D.T., 2021. A 200-million-year delay in permanent atmospheric oxygenation. Nature 592, 232–236. https://doi.org/10.1038/s41586-021-03393-7

Poulton, S.W., Raiswell, R., 2002. The low-temperature geochemical cycle of iron: From continental fluxes to marine sediment deposition. Am J Sci 302, 774–805. https://doi.org/10.2475/ajs.302.9.774

Ren, H.-T., Jia, S.-Y., Wu, S.-H., Liu, Y., Hua, C., Han, X., 2013. Abiotic oxidation of Mn(II) induced oxidation and mobilization of As(III) in the presence of magnetite and hematite. J Hazard Mater 254, 89–97. https://doi.org/10.1016/j.jhazmat.2013.03.022

Rouxel, O.J., Bekker, A., Edwards, K.J., 2005. Iron Isotope Constraints on the Archean and Paleoproterozoic Ocean Redox State. Science 307, 1088 1091. https://doi.org/10.1126/science.1105692

Satkoski, A.M., Beukes, N.J., Li, W., Beard, B.L., Johnson, C.M., 2015. A redox-stratified ocean 3.2 billion years ago. Earth Planet Sc Lett 430, 43 53. https://doi.org/10.1016/j.epsl.2015.08.007

Schaefer, M.V., Handler, R.M., Scherer, M.M., 2017. Fe(II) reduction of pyrolusite (β-MnO2) and secondary mineral evolution. Geochem T 18, 7. https://doi.org/10.1186/s12932-017-0045-0

Schier, K., Bau, M., Smith, A.J.B., Beukes, N.J., Coetzee, L.L., Viehmann, S., 2020. Chemical evolution of seawater in the Transvaal Ocean between 2426 Ma (Ongeluk Large Igneous Province) and 2413 Ma ago (Kalahari Manganese Field). Gondwana Res 88, 373–388. https://doi.org/10.1016/j.gr.2020.09.001

Schröder, S., Bedorf, D., Beukes, N.J., Gutzmer, J., 2011. From BIF to red beds: Sedimentology and sequence stratigraphy of the Paleoproterozoic Koegas Subgroup (South Africa). Sediment Geol 236, 25–44. https://doi.org/10.1016/j.sedgeo.2010.11.007

Shih, P.M., Hemp, J., Ward, L.M., Matzke, N.J., Fischer, W.W., 2016. Crown group Oxyphotobacteria postdate the rise of oxygen. Geobiology 15, 19–29. https://doi.org/10.1111/gbi.12200

Siahi, M., Tsikos, H., Rafuza, S., Oonk, P.B.H., Mhlanga, X.R., Niekerk, D. van, Mason, P.R.D., Harris, C., 2020. Insights into the processes and controls on the absolute abundance and distribution of manganese in Precambrian iron formations. Precambrian Res 350, 105878. https://doi.org/10.1016/j.precamres.2020.105878

Slotznick, S.P., Johnson, J.E., Rasmussen, B., Raub, T.D., Webb, S.M., Zi, J.-W., Kirschvink, J.L., Fischer, W.W., 2022. Reexamination of 2.5-Ga "whiff" of oxygen interval points to anoxic ocean before GOE. Sci Adv 8, eabj7190. https://doi.org/10.1126/sciadv.abj7190

Smith, A.J.B., 2018. The Iron Formations of Southern Africa, in: Siegesmund, S., Basei, M.A.S., Oyhantçabal, P., Oriolo, S. (Eds.), Geology of Southwest Gondwanda, Regional Geology Reviews. pp. 469–491. https://doi.org/10.1007/978-3-319-68920-3_17

Smith, A.J.B., Beukes, N.J., 2023. The paleoenvironmental implications of pre-Great Oxidation Event manganese deposition in the Mesoarchean Ijzermijn Iron Formation Bed, Mozaan Group, Pongola Supergroup, South Africa. Precambrian Res 384, 106922. https://doi.org/10.1016/j.precamres.2022.106922

Smith, A.J.B., Beukes, N.J., 2016. Palaeoproterozoic banded iron formation hosted high-grade hematite iron ore deposits of the Transvaal Supergroup, South Africa. Episodes 39, 269–284. https://doi.org/10.18814/epiiugs/2016/v39i2/95778

Smith, A.J.B., Beukes, N.J., Gutzmer, J., 2013. The Composition and Depositional Environments of Mesoarchean Iron Formations of the West Rand Group of the Witwatersrand Supergroup, South Africa. Econ Geol 108, 111–134. https://doi.org/10.2113/econgeo.108.1.111

Smith, A.J.B., Beukes, N.J., Gutzmer, J., Czaja, A.D., Johnson, C.M., Nhleko, N., 2017. Oncoidal granular iron formation in the Mesoarchaean Pongola Supergroup, southern Africa: Textural and geochemical evidence for biological activity during iron deposition. Geobiology 15, 731 749. https://doi.org/10.1111/gbi.12248

Smith, A.J.B., Beukes, N.J., Cochrane, J.M., Gutzmer, J., 2023. Manganese carbonate-bearing mudstone of the Witwatersrand-Mozaan succession in southern Africa as evidence for bacterial manganese respiration and availability of free molecular oxygen in Mesoarchean oceans. S Sfr J Geol 126. https://doi.org/10.25131/sajg.126.0005

Sperling, E.A., Wolock, C.J., Morgan, A.S., Gill, B.C., Kunzmann, M., Halverson, G.P., Macdonald, F.A., Knoll, A.H., Johnston, D.T., 2015. Statistical analysis of iron geochemical data suggests limited late Proterozoic oxygenation. Nature 523, 451 454. https://doi.org/10.1038/nature14589

Spinks, S.C., Sperling, E.A., Thorne, R.L., LaFountain, F., White, A.J.R., Armstrong, J., Woltering, M., Tyler, I.M., 2023. Mesoproterozoic surface oxygenation accompanied major sedimentary manganese deposition at 1.4 and 1.1 Ga. Geobiology 21, 28–43. https://doi.org/10.1111/gbi.12524

Stolper, D.A., Keller, C.B., 2018. A record of deep-ocean dissolved O2 from the oxidation state of iron in submarine basalts. Nature 33, 1 11. https://doi.org/10.1038/nature25009

Stumm, W., Morgan, J., 1996. Aquatic Chemistry, Chemical Equilbria and rates in natural waters, 3rd ed. John Wiley & Sons, Inc., New York.

Su, G., Zopfi, J., Yao, H., Steinle, L., Niemann, H., Lehmann, M.F., 2020. Manganese/iron-supported sulfate-dependent anaerobic oxidation of methane by archaea in lake sediments. Limnol Oceanogr 65, 863–875. https://doi.org/10.1002/lno.11354

Sumner, D.Y., Bowring, S.A., 1996. U–Pb geochronologic constraints on deposition of the Campbellrand Subgroup, Transvaal Supergroup, South Africa. Precambrian Res 79, 25–35. https://doi.org/10.1016/0301-9268(95)00086-0

Sunda, W.G., Huntsman, S.A., 1994. Photoreduction of manganese oxides in seawater. Mar Chem 46, 133–152. https://doi.org/10.1016/0304-4203(94)90051-5

Sunda, W.G., Huntsman, S.A., 1988. Effect of sunlight on redox cycles of manganese in the southwestern Sargasso Sea. Deep Sea Res Part Oceanogr Res Pap 35, 1297–1317. https://doi.org/10.1016/0198-0149(88)90084-2

SUNDBY, B., 1977. Manganese-rich particulate matter in a coastal marine environment. Nature 270, 417–419. https://doi.org/10.1038/270417a0

Swanner, E.D., Lambrecht, N., Wittkop, C., Harding, C., Katsev, S., Torgeson, J., Poulton, S.W., 2020. The biogeochemistry of ferruginous lakes and past ferruginous oceans. Earth-sci Rev 211, 103430. https://doi.org/10.1016/j.earscirev.2020.103430

Tebo, B.M., Johnson, H.A., McCarthy, J.K., Templeton, A.S., 2005. Geomicrobiology of manganese(II) oxidation. Trends Microbiol 13, 421–428. https://doi.org/10.1016/j.tim.2005.07.009

Thamdrup, B., Glud, R.N., Hansen, J.W., 1994. Manganese oxidation and in situ manganese fluxes from a coastal sediment. Geochim Cosmochim Ac 58, 2563–2570. https://doi.org/10.1016/0016-7037(94)90032-9

Tonkin, J.W., Balistrieri, L.S., Murray, J.W., 2004. Modeling sorption of divalent metal cations on hydrous manganese oxide using the diffuse double layer model. Appl Geochem 19, 29–53. https://doi.org/10.1016/s0883-2927(03)00115-x

Tsikos, H., Beukes, N.J., Moore, J.M., Harris, C., 2003. Deposition, Diagenesis, and Secondary Enrichment of Metals in the Paleoproterozoic Hotazel Iron Formation, Kalahari Manganese Field, South Africa. Econ Geol 98, 1449 1462. https://doi.org/10.2113/gsecongeo.98.7.1449

Tsikos, H., Matthews, A., Erel, Y., Moore, J.M., 2010. Iron isotopes constrain biogeochemical redox cycling of iron and manganese in a Palaeoproterozoic stratified basin. Earth Planet Sc Lett 298, 125–134. https://doi.org/10.1016/j.epsl.2010.07.032

Tsikos, H., Moore, J.M., 1997. Petrography and geochemistry of the Paleoproterozoic Hotazel Iron-Formation, Kalahari manganese field, South Africa; implications for Precambrian manganese metallogenesis. Econ Geol 92, 87 97. https://doi.org/10.2113/gsecongeo.92.1.87

Tsikos, H., Siahi, M., Rafuza, S., Mhlanga, X.R., Oonk, P.B.H., Papadopoulos, V., Boyce, A.J., Mason, P.R.D., Harris, C., Gröcke, D.R., Lyons, T.W., 2022. Carbon isotope stratigraphy of Precambrian iron formations and possible significance for the early biological pump. Gondwana Res 109, 416–428. https://doi.org/10.1016/j.gr.2022.05.007

Van Cappellen, P.V., Viollier, E., Roychoudhury, A., Clark, L., Ingall, E., Lowe, K., Dichristina, T., 1998. Biogeochemical Cycles of Manganese and Iron at the Oxic−Anoxic Transition of a Stratified Marine Basin (Orca Basin, Gulf of Mexico). Environ Sci Technol 32, 2931–2939. https://doi.org/10.1021/es980307m

Van Cappellen, P.V., Wang, Y., 1996. Cycling of iron and manganese in surface sediments; a general theory for the coupled transport and reaction of carbon, oxygen, nitrogen, sulfur, iron, and manganese. Am J Sci 296, 197–243. https://doi.org/10.2475/ajs.296.3.197

Wang, C., Robbins, L.J., Planavsky, N.J., Beukes, N.J., Patry, L.A., Lalonde, S.V., Lechte, M.A., Asael, D., Reinhard, C.T., Zhang, L., Konhauser, K.O., 2022. Archean to early Paleoproterozoic iron formations document a transition in iron oxidation mechanisms. Geochim Cosmochim Ac. https://doi.org/10.1016/j.gca.2022.12.002

Warke, M.R., Rocco, T.D., Zerkle, A.L., Lepland, A., Prave, A.R., Martin, A.P., Ueno, Y., Condon, D.J., Claire, M.W., 2020. The Great Oxidation Event preceded a Paleoproterozoic "snowball Earth." Proc National Acad Sci 117, 13314–13320. https://doi.org/10.1073/pnas.2003090117

Wittkop, C., Swanner, E.D., Grengs, A., Lambrecht, N., Fakhraee, M., Myrbo, A., Bray, A.W., Poulton, S.W., Katsev, S., 2020. Evaluating a primary carbonate pathway for manganese enrichments in reducing environments. Earth Planet Sc Lett 538, 116201. https://doi.org/10.1016/j.epsl.2020.116201

Wittkop, C., Teranes, J., Lubenow, B., Dean, W.E., 2014. Carbon- and oxygen-stable isotopic signatures of methanogenesis, temperature, and water column stratification in Holocene siderite varves. Chem Geol 389, 153–166. https://doi.org/10.1016/j.chemgeo.2014.09.016

Yamagata, N., Iwashima, K., 1963. Monitoring of Sea-Water for Important Radioisotopes Released by Nuclear Reactors. Nature 200, 52–52. https://doi.org/10.1038/200052a0

Yan, H., Pi, D., Jiang, S.-Y., Hao, W., Cui, H., Robbins, L.J., Mänd, K., Li, L., Planavsky, N.J., Konhauser, K.O., 2020. Hydrothermally induced 34S enrichment in pyrite as an alternative explanation of the Late-Devonian sulfur isotope excursion in South China. Geochim Cosmochim Ac. https://doi.org/10.1016/j.gca.2020.05.017

Yan, H., Pi, D.-H., Jiang, S.-Y., Mao, J., Xu, L., Yang, X., Hao, W., Mänd, K., Li, L., Konhauser, K.O., Robbins, L.J., 2022. Mineral paragenesis in Paleozoic manganese ore deposits: Depositional versus post-depositional formation processes. Geochim Cosmochim Ac 325, 65–86. https://doi.org/10.1016/j.gca.2022.03.030

1498 Yu, H., Leadbetter, J.R., 2020. Bacterial chemolithoautotrophy via manganese oxidation. Nature
1499 583, 453–458. https://doi.org/10.1038/s41586-020-2468-5

1500 Zerkle, A.L., Mikhail, S., 2017. The geobiological nitrogen cycle: From microbes to the mantle.
1501 Geobiology 15, 343–352. https://doi.org/10.1111/gbi.12228

1502 Zerkle, A.L., Poulton, S.W., Newton, R.J., Mettam, C., Claire, M.W., Bekker, A., Junium, C.K.,
1503 2017. Onset of the aerobic nitrogen cycle during the Great Oxidation Event. Nature 542, 465–
1504 467. https://doi.org/10.1038/nature20826